UNIVERSITY OF TWENTE.

# Isolation of Hepatocellular carcinoma (HCC) derived extracellular vesicles

Using click-chemistry conjugated immunomagnetic beads

Master thesis by Sven Mentink (Student M-BME)
Department of Medical cell Biophysics (MCBP)
Student number (s1937499)

***Exam committee:***
*Richell Booijink, Msc.*
*Dr. Ruchi Bansal*
*Prof. Dr. Ir. Pascal Jonkheijm*

# Abstract

Hepatocellular carcinoma (HCC) is one of the top five most common malignant tumour types in the western world. The asymptomatic nature of early stage HCC leads to an issue that most patients are diagnosed at late stages of the disease, in which treatments are far less effective. Tumour derived extracellular vesicles (EVs) have been identified as novel liquid biopsy markers for early diagnosis and prognosis in HCC. However, current methods are insufficient for specific isolation of these HCC derived EVs. Here, we aim to develop a system that is capable of specifically capturing HCC derived EVs from conditioned cell medium. By combining different EV characterisation techniques initial presence of HCC derived EVs in conditioned cell medium could be confirmed. The developed capturing system is based on magnetic beads covalently conjugated to antibodies by Tetrazine (Tz) trans-cyclooctyne (TCO) mediated “click” reaction. Fluorescence activated cell sorting (FACS) and microscopy confirmed successful conjugation of subparts of the system, by making use of the inherent fluorescent properties of Tz. Subsequently, by successful staining of EVs with Calcein, FACS showed the capturing of HCC derived EVs from HepG2 cell conditioned medium.

# Table of contents

# 1. Theoretical background

## 1.1. Problem statement (HCC)

Hepatocellular carcinoma (HCC) is one of the top five most common malignant tumour types in the western world with an ever increasing incidence and mortality [1]. The survival rate of HCC is very low with a 5-year survival rate among patients of less than 20% [1]. HCC has multiple different causes and risk factors associated with it. Most prominent of these is that HCC can develop from an underlying (end-stage) liver disease. Liver disease, on its turn, can be caused by viral infections (hepatitis B and C), metabolic and immune diseases or abuse of toxic substances such as alcohol [2].

Specifically detecting the progression of these underlying diseases to HCC can be challenging. This is primarily due to the asymptomatic nature of the early stages of HCC. However, it is important to note that the difficulty lies in detecting HCC itself, as well as identifying the underlying diseases that may lead to its development. Both aspects can be challenging to detect and diagnose accurately. The asymptomatic nature in early stage HCC leads to an issue that most patients are diagnosed with late stage HCC, in which treatment effectiveness is way lower than treatment in preceding stages [3].

Currently, most patients are diagnosed with HCC due to surveillance programs focussed on people with a high risk of developing the disease. Individuals considered to be at high risk of developing HCC are people with chronic hepatitis (B and C), hemochromatosis, cirrhosis, NAFLD, NASH, or other underlying (chronic) liver diseases [4]. Liver ultrasonography and serum α fetoprotein detection are the two most used methods in HCC surveillance for people who are at risk [5]. Liver ultrasonography is widely available, relatively cheap and accepted by most patients. However its sensitivity (40-80%) and specificity (82-100%) for detection of HCC is far from optimal [6]. Factors that play a role in the poor sensitivity include variability in operator experience, amount of steatosis and fat in the liver, and size of the liver lesion.

Alpha fetoprotein (AFP) is a plasma protein (70kDa) mainly produced in the developing liver of a foetus during pregnancy. Elevated serum AFP levels are also associated with HCC and used as a surveillance program for high at risk individuals [7]. However AFP levels are not elevated in all HCC patients, being elevated only in 60-70% of HCC patients. Furthermore, other non-tumorigenic causes can also lead to elevated AFP levels, leading to a specificity of around 80% to 94% (20 ng/mL cut-off) [8]. Some researchers (Zhang et, al. [8]), have evaluated the effect of different cut-off concentrations of AFP, in most cases trading specificity for sensitivity when increasing cut-off concentrations. Although they did find an optimum cut-off of 400 ng/mL, the is still a lot of room for improvement when you look at the sensitivity (32%).

As these current screening methods are insufficient/suboptimal in the early diagnosis of HCC, new methods are being developed for better screening and diagnosis. There are several advances made in the field of diagnostic imaging and radiology, such as the LI-RADS system, hepatocyte-specific contrast agents for MRI and contrast enhanced ultrasound [9]. However, the focus of this research will rely on the highly promising field of liquid biopsies. Novel biomarkers and techniques to detect these biomarkers could revolutionize the way in which HCC is diagnosed.

## 1.2. Liquid biopsy

In contrast to the traditional tissue biopsy, in which a piece of the tumour is extracted from the patient for analysis, liquid biopsy focusses on traces/metabolites of the tumour cells in the bodily fluids of patients [10]. In this way, liquid biopsy provides a minimally invasive way to measure biomarkers of a disease. The assessment of these biomarkers can be helpful in disease diagnosis, monitoring and prognosis of the disease. As displayed in Figure 1, one possible liquid biopsy that can be helpful in diagnosis of HCC would be biopsy using blood plasma. Interesting components that can be analysed in the blood of HCC patients would be tumour associated proteins, extracellular vesicles, circulating tumour cells (CTCs), tumour associated nucleic acids and tumour secreted metabolomics.

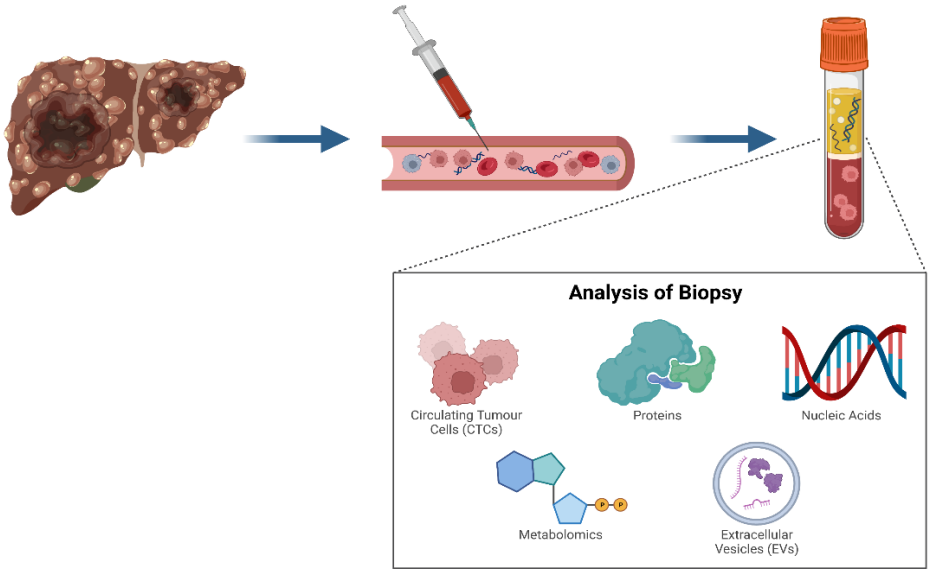


*Figure 1: Schematic representation of the process of liquid biopsy, focusing on the extraction of a liquid biopsy sample and its constituents (image was made using Biorender).*

Liquid biopsies have several advantages over conventional tissue biopsies. Besides lower invasiveness it allows for detection of spatial and temporal differences intratumorally, it is faster and generally cheaper [10]. However, a disadvantage of liquid biopsies is that in most cases they are not clinically validated.

In HCC, measuring plasma AFP concentration is a clinically validated liquid biopsy technique for diagnosis. As of the earlier mentioned limitations in sensitivity and specificity of this diagnosis method, research has tried to identify other tumour associated proteins. In Table 1, other protein biomarkers that were evaluated in liquid biopsies for the detection of HCC are summarized.

*Table 1: Biomarker proteins in HCC. Functions, advantages and limitations.*

| Protein | Function | Relevance | Limitation(s) | Source |
|---|---|---|---|---|
| Alpha-Fetoprotein-L3 (AFP-L3) | Involved in foetal development. | Superior detection in malignant tumours (high specificity) compared to AFP. | Low sensitivity | [11] |
| Des-gamma-carboxy Prothrombin (DCP) | Important for blood clotting. Involved in tumour cell proliferation and angiogenesis. | Better detection of early stage HCC compared to AFP and AFP-L3. | Low sensitivity | [12] |
| Glypican-3 (GPC3) | Plays a role in cell growth and development. | Elevated in HCC liver cells but not in healthy liver cells or pathological cells with hepatitis/cirrhosis. | Effect is more prominent in tissue biopsy rather than in liquid biopsy. | [11] |
| Cytokeratin 19 (CK19) | Provide structural support to cells and maintain cellular integrity. | Biomarker for patients with poor prognosis. | Not sufficient as a diagnostic tool by itself. | [12] |
| Golgi protein 73 (GP73) | Involved in protein trafficking, Golgi structure maintenance, and cell adhesion. | Indicator of recurrence of HCC; Elevated in several liver diseases. | Larger studies needed to confirm surveillance potential. | [11] |
| Midkine (MDK) | Involved in various biological processes, including cell growth, survival, and differentiation. | High solubility leads to an easily measurable biomarker in the circulation. | Relatively low specificity. | [13] |
| Osteopontin (OPN) | Involved in various physiological and pathological processes, including bone metabolism, tissue remodelling, immune response, and cancer progression. | Potential in early diagnosis of HCC for patients with nodules < 2cm. | Elevated expression in a lot of different cancer types. | [12,14] |
| Serum Squamous Cell Carcinoma Antigen (SCCA) and immunoglobulin M isoform (SCCA-IgM) | Play a role in tumour growth, invasion, and metastasis. | Elevated expression is associated to HCC development; SCCA-IgM in combination with AFP has diagnostic potential for early HCC. | Biomarkers with moderately diagnostic capabilities by themselves | [12,15] |

Although there is a lot of research done and ongoing towards proteins in liquid biopsies, Table 1 implies that looking solely at protein levels is insufficient for the accurate detection of HCC. As displayed in Figure 1, liquid biopsies also contain information on metabolomics, circulating tumour cells (CTCs), nucleic acids and extracellular vesicles (EVs). Due to their higher stability compared to

nucleotides and metabolomics, and their higher availability compared to CTCs the rest of this research will focus on the diagnostic potential of EVs. However, choosing one does not cancel out the other as EVs hold information about nucleotides and metabolomics inside their cargoes as well.

## 1.3. Extracellular vesicles

Extracellular vesicles (EVs) are particles made up of lipid bilayer structure with sizes ranging from 30nm to 5000nm, although some researchers claim that some vesicles exceeding 5000nm should also still be considered as EVs [16,22]. EVs can be divided into subtypes based on biogenesis, release pathways, size, content, and function [19]. Table 2, summarizes different subtypes of EVs found in literature. The vesicles can contain proteins, lipids, nucleic acids and are excreted by both normal cells as by cancerous cells.

*Table 2: Extracellular vesicle subtypes used in scientific literature. Nomenclature, size ranges and biogenesis.*

| Classification | Size range lower limit (nm) | Size range upper limit (nm) | Biogenesis | Source |
|---|---|---|---|---|
| Exomeres | 0 | 50 | Unknown | [16,17] |
| Small exosomes | 60 | 80 | Intraluminal vesicles are released when multivesicular bodies fuse with the plasma membrane | [16] |
| Exosomes | 30-50 | 100-200 | Intraluminal vesicles are released when multivesicular bodies fuse with the plasma membrane | [18–23] |
| Large exosomes | 90 | 120 | Intraluminal vesicles are released when multivesicular bodies fuse with the plasma membrane | [16] |
| Microvesicles | 50-100 | 1000 | Vesicles originate from direct membrane budding of the plasma membrane | [16,18–23] |
| Migrasomes | 500 | 3000 | Vesicles originate from migrating cells and are excreted from the tips of their retraction fibres | [16,20] |
| Large oncosomes | 1000 | 10,000 | Originate from membrane shedding of cancer cells with an amoeboid phenotype | [16,22] |
| Apoptotic bodies | 50-1000 | 2000-5000 | Vesicles originate from plasma membrane separation from the cytoskeleton during the apoptosis process | [18,19,21–23] |

The variety in EV subtypes can cause confusion and misplaced translation of the research results. To prevent this phenomenon from happening, the International Society for Extracellular Vesicles (ISEV) recommends researchers to clearly define the nomenclature used in their paper/thesis [24]. To provide clarity and easy readability, in this thesis EVs are defined as “particles made up of lipid

bilayer structure with sizes ranging from 30nm to 5000nm", as mentioned earlier in this section. Furthermore distinction in EVs will be made based upon their cellular origins, i.e. HCC derived EVs being EVs derived from hepatocellular carcinoma cells. However in some cases, when elaborating techniques/papers by other researchers the nomenclature of Table 2, could be helpful.

In recent years, the role of EVs in cancer initiation, development and progression has become more evident. For example, elevated levels of larger (size between 1000nm-12000nm) tumour derived extracellular vesicles (tdEVs) in the blood of patients showed to be a prognostic marker for survival in various metastatic cancers [25]. Considering that these larger tdEVs are expected to be only a small percentage (<1%) of the total tdEV population [25], one could imagine the impact in cancer research when total tdEV populations can be evaluated. Next to the amount of EVs, their cargo can also provide valuable information used in diagnosis, prognosis and treatments. As mentioned earlier EVs can contain proteins, lipids, nucleic acids and metabolites. The cargo of EVs is dependent on their cellular origin, variating per cell type and disease state. For example EVs from healthy hepatocytes might be different compared to HCC derived hepatocytes, as will be discussed later this chapter. In Figure 2, a visual representation is provided with common EV cargoes [26].

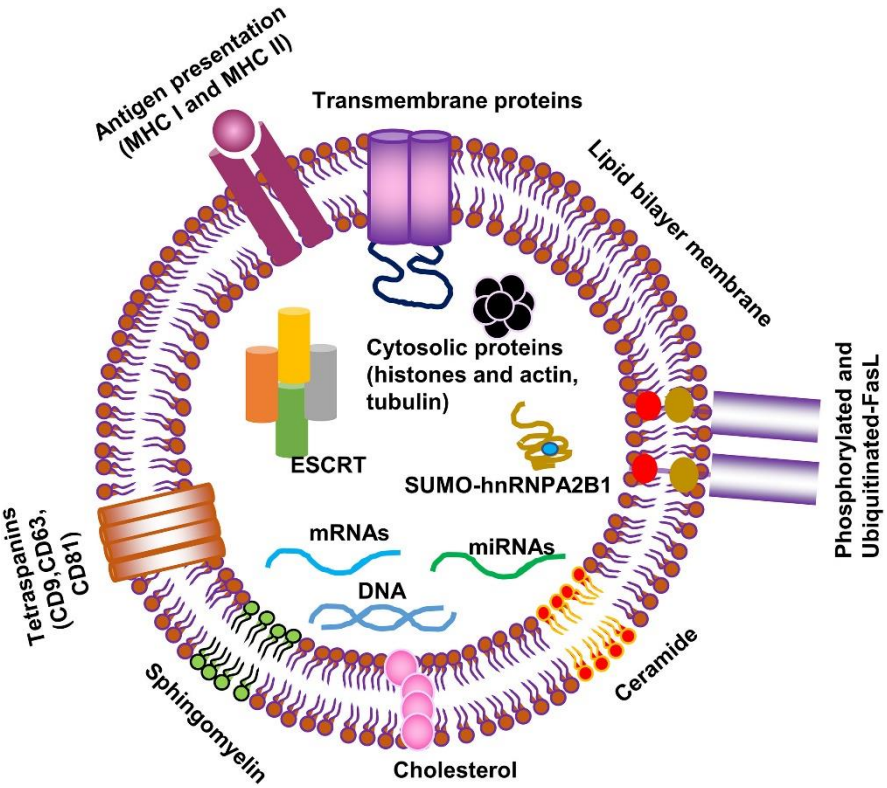


*Figure 2: Schematical representation of an extracellular vesicle (EV) and its cargo. EVs contain a wide range of cargoes such as nucleotides (miRNA, mRNA, DNA) and cytosolic proteins (ESCRT, SUMO-hnRNPA2B1). Furthermore, transmembrane proteins are anchored in their lipid bilayer membrane together with some functional chemical groups [26].*

## 1.4. Isolating extracellular vesicles

The limiting factor in using EVs as liquid biopsy markers lies in the difficulty to isolate them from other constituents of bodily fluids. Conventional methods to isolate EVs focus on separation based on size and density [18,19]. In tangential flow filtration (TFF) a column with membrane fibers is used to filter out EVs based on size [27,28]. In ultracentrifugation high-speed centrifugal forces are used to separate EVs based on size and density, with the end result being a formed pellet of EVs [29]. In density gradient centrifugation separation is based on the relative density of the EVs to a fluid medium they are dispersed in [29]. Precipitation methods can vary from specific polymers to solubilisation agents that specifically precipitate EVs in a sample [30]. Methods based on immunocapture use antibodies to selectively bind EVs to nanoparticles or other substrates [31]. Microfluidic based -techniques are often combined with immunocapture or use chip-surface manipulation and flow rates to isolate EVs in microfluidic channels [32]. Finally, size-exclusion chromatography (SEC) is a separation technique based on the time EVs spend to cross a column with a gel matrix, which is dependent on their size and molecular weight [22]. In Table 3, the advantages and limitations of the most common techniques for isolating EVs will be discussed.

*Table 3: Different types of extracellular vesicle isolation methods. Advantages and Limitations.*

| Technique | Advantage(s) | Limitation(s) | Source |
|---|---|---|---|
| Ultracentrifugation (UC) | Well-established method, can isolate different size ranges of EVs, can concentrate EVs efficiently. | Potentially alters EV integrity, can cause agglomeration of EVs. Co-isolation of non-EVs. | [29] |
| Density gradient centrifugation (DGC) | Can obtain highly purified EV fractions. | Potentially alters EV integrity, can cause agglomeration of EVs, high loss of EVs during process. | [29] |
| Tangential flow filtration (TFF) | Scalable for large volumes. Easy to perform. Does not separate EV subpopulations (can also be a limitation based on intended use). | Clogging of the membrane, resulting in a loss of EVs. Co-isolation of non-EVs. | [27,28] |
| Precipitation methods | High yield of EVs, easy to perform | Co-precipitation of non-EVs. Potentially alters EV integrity. | [30] |
| Immunocapture | Highly specific and can lead to high purity. Can isolate subtypes of EVs. | Potential loss of non-targeted EVs, variable efficiency due to antibody. | [31] |
| Microfluidic-based techniques | Potential for high-throughput isolation. | Limited availability of commercial platforms, need optimization for specific applications. | [32] |
| Size-exclusion chromatography (SEC) | Minimal damage to EVs. Efficient separation based on size. | Lower recovery of small EVs. Co-isolation of non-EVs. | [22,33] |

## 1.5 The role of hepatocytes and EVs in HCC

The prognostic and diagnostic potential of EV based liquid biopsies could, when captured and isolated more efficiently, be a way to fill in the knowledge gap in HCC diagnosis, monitoring and prognosis. To identify the real value of EV based liquid biopsies for specifically HCC, it is necessary to understand the role EVs play in the development of HCC. This is important as EVs often vary in counts and cargo between various types of cancer. In this research, there will be a focus on the role of hepatocytes and hepatocyte derived EVs in HCC. Hepatocytes are the main functional cells of the liver, comprising approximately 80% of its cellular mass [34]. They are specialized epithelial cells responsible for carrying out various functions essential for liver health and metabolism. Hepatocytes play a crucial role in several physiological processes such as detoxification, protein synthesis, bile production, lipid and drug metabolism as well as providing a storage site for minerals, vitamins and glycogen [34].

In HCC, genetic and epigenetic alterations occur in hepatocytes, leading to uncontrolled cell growth and the formation of a tumour mass within the liver. Although there is little to no data specific on how this alters hepatocyte derived EVs (this is why we aim to isolate them in this research), there is data on how EV cargoes can influence pathophysiology in HCC. Disruptions in cellular communication, in HCC, can occur by many different cargoes from different cell populations; such as hepatocytes (healthy or tumour), stellate cells, and immune cells [35]. These disruptions in important communication pathways can lead to pathogenic processes such as angiogenesis, cancer cell proliferation, cancer metastasis and protect the tumour against recognition by immune cells [35]. The exact mechanism of how these EVs alter these pathogenic processes falls out of the scope of this research however, using Figure 3, the shear complexity of the influence of EVs on pathogenic processes can be visualised.

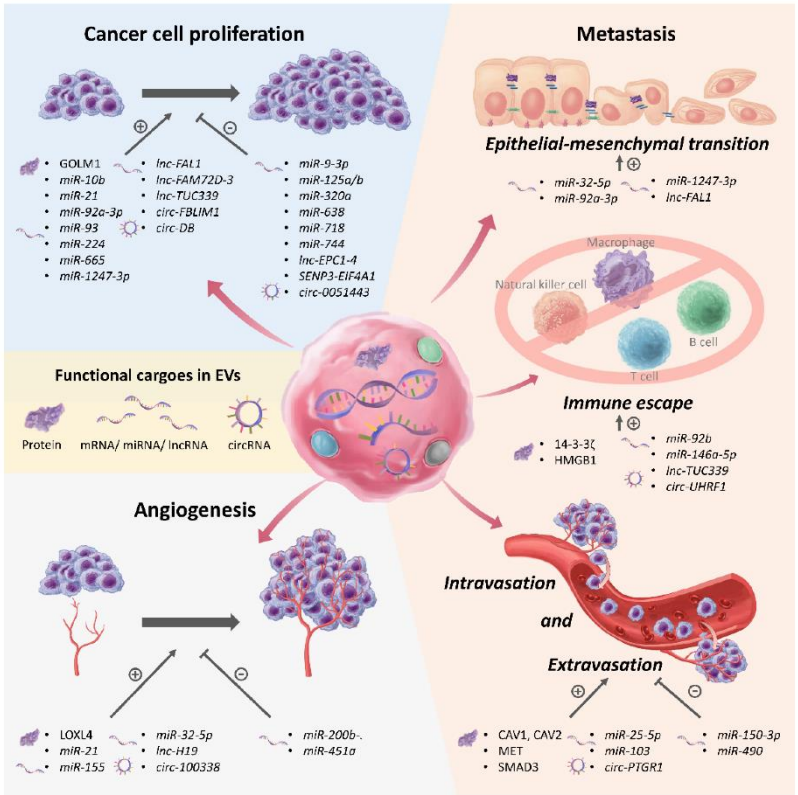


*Figure 3: EVs have emerged as important mediators in the progression of HCC. Studies have revealed that EVs play a regulatory role in key processes such as cancer cell proliferation, angiogenesis, metastasis, immune escape, and intravasation/extravasation. These functional effects are attributed to EV cargoes. This visualises the complex influence that EVs have on HCC [35].*

# 2. Aim and objectives

In this thesis, the aim is to develop a system that is capable of specifically capturing HCC derived EVs from conditioned cell medium.

The intent is to achieve the aim through completion of the following objectives:

1) Confirm that the initial sample of conditioned medium contains HCC derived EVs. To complete this objective, a combination of different EV characterisation techniques will be used to analyse particles in the medium based on size, morphology, counts, proteomics and enzyme activity.

2) Ensure successful conjugation of the subparts of the capturing system. By taking advantage of inherent auto fluorescent properties, FACS and microscopy can be used to confirm or deny successful conjugation.

3) Establish a way to confirm that the system actually captures the HCC derived EVs from the medium. To achieve this objective, a fluorescent staining will be applied to the HCC derived EVs. This staining will make it possible to detect captured (conjugated) HCC derived EVs to the capturing system by FACS.

Gaining more knowledge into the capturing efficiency of the system and using this knowledge to optimize the capturing system were possible. Several tests will be performed to analyse the capturing efficiency. Furthermore, additional features such as cleavable groups for controlled release after capture and sorting of the capturing system to increase purity of successful conjugated subparts will be explored and tested.

# 3. The system: Click-chemistry conjugated immunomagnetic beads

## 3.1 Concept

The demand for novel HCC liquid biopsy methods providing both high specificity and sensitivity combined with the diagnostic potential of EVs, results in the need for a special type of system. It is important to note that the development of a system for isolating and characterizing EVs from biofluids is a complex process that involves multiple steps, and different methods and techniques can be combined to optimize the performance. The system should be EV-specific, easily accessible, preserve EV-integrity and be consistent. Additionally, since there is no generally accepted method of EV characterisation the system would need several measurable parameters, in-process controls, to verify that it actually captures EVs. In this thesis the system that will be used is based upon click-chemistry conjugated immunomagnetic beads, as visualised in Figure 4.

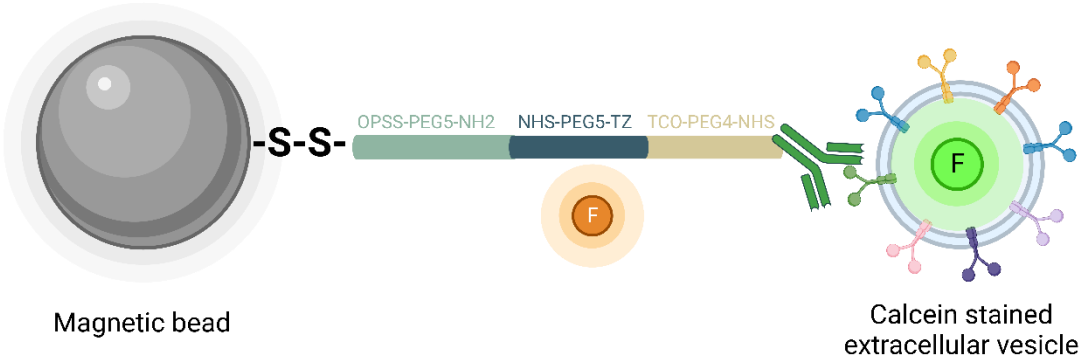


*Figure 4: Completely conjugated system for capturing HCC derived EVs. The system is made up of several different subparts. The two endpoints of the system are the magnetic beads and the Calcein stained EVs. Circles, with the letter F, indicate fluorescent activity of the Tetrazine group and the Calcein staining (image was made using Biorender).*

## 3.2 Design

The design of the system will be divided into four different subchapters. Each of the subchapters covers an essential step in the conjugation of the capturing system.

### 3.2.1 Obtaining Tetrazine functionalised magnetic beads

The capturing system consists of two main parts that will be optimized for HCC derived EVs. The first elementary part of the system consists of AccuBead™ Thiol Magnetic Beads, made up of silica and iron oxide. As their name implies these magnetic beads are functionalised with thiol groups, enabling easy conjugation to other (bio)molecules [36]. To decrease steric hinderance (hypothesis) and ensure high capture efficiency, a linker is conjugated to the magnetic nanoparticles, this linker contains Polyethylene glycol (PEG) spacer units. The linker group originates from two separate successive reactions.

The first reaction (Figure 5) is called the thiol-pyridyl disulphide exchange reaction [37]. In this reaction the thiol functionalised beads react with the molecule OPSS-PEG5-NHS (pH=7), resulting in the formation of a sulphide bridge and splitting of a molecule called pyridine – 2 – thione. This reaction can be seen in Figure 5. It is important to note that the formed disulphide bridge can be cleaved-off again in a reaction with Dithiothreitol (DTT).

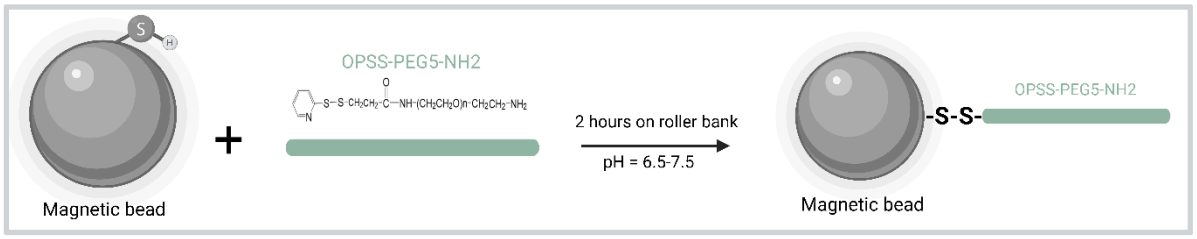


*Figure 5: Schematic representation of the reaction of OPSS-PEG5-NH2 with thiol functionalised magnetic beads forming a disulphide bond. The reactants were incubated for 2 hours on a roller mixer at neutral pH (image was made using Biorender).*

In a second reaction, the NHS molecule from the Bead-OPSS-PEG5-NHS construct is able to react with an added 6-Methyl-Tetrazine-PEG5-NHS ester (pH=8.5) and form a stable amide bond. After this conjugation reaction the first elementary part of the system is complete. The part consist of Tetrazine (Tz) – functionalised magnetic beads with a reduceable disulphide linkage in between. The second part of the functionalisation is shown in Figure 6.

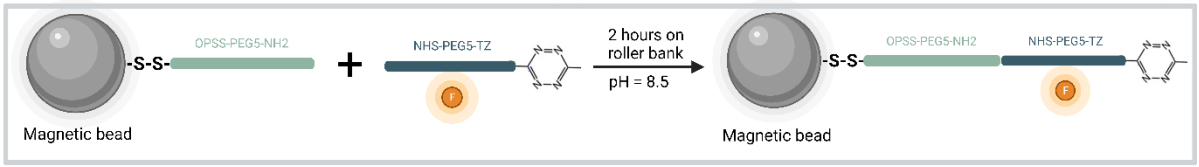


*Figure 6: Schematic representation of the reaction of OPSS functionalised beads with TZ-PEG5-NHS forming an amide bond. The reactants were incubated for 2 hours on a roller mixer at slightly basic pH. The circle, with the letter F, indicates fluorescent activity of the Tz group in the Pe channel (ex 488 ; em 585/40) (image was made using Biorender).*

This reaction takes place at pH=8.5, as the optimal pH to react N-hydroxysuccinimide (NHS) with amino ($NH_2$) groups typically ranges between pH 7 and pH 9 [38]. At a pH lower than 7, the amine groups may exist predominantly in their protonated form ($NH_3^+$), which can hinder the reaction with NHS. On the other hand, at a pH higher than 9, the NHS molecule itself may become less stable, resulting in hydrolysis and reduced reactivity.

### 3.2.2 Obtaining Trans-cyclooctene functionalised antibodies

The second elementary part of the capturing system consists of an antibody that is used to capture the EVs, in this case Epithelial Cell Adhesion Molecule (EpCAM) or Asialoglycoprotein Receptor 1 (ASGR1).

EpCAM is a cell surface glycoprotein that is frequently overexpressed in epithelial-derived cancers, such as HCC [39]. The transmembrane protein has been used in capturing systems before, mainly to capture and isolate circulating tumour cells or tdEVs [25,40]. Most solid cancer types are of epithelial origin, while normal blood cells have a mesenchymal phenotype, meaning that cancer cells express EpCAM, while normal blood cells do not. This difference enables separation based on EpCAM antibody mediated immunocapture. Fortunately, EpCAM is not only expressed in cancer cells but also in its excreted tdEVs. Research has shown that in HCC, EpCAM expression can be a useful biomarker in liquid biopsies [41].

ASGR1, sometimes also depicted as ASGPR1, is part of a cell surface receptor that is primarily expressed on hepatocytes, which are the main functional cells of the liver [42]. Incorporating ASGR1 into such an immunocapturing system harnesses its high specificity for hepatocytes, enabling the selective capture of HCC derived EVs from a mixture of EVs released by various cell types. Similar to

EpCAM, ASGR1 is expressed in HCC derived EVs and can be used as a biomarker in liquid biopsies [41].

To facilitate strong and specific conjugation to the first elementary part of the system (Beads-OPSS-Tz), the antibody is functionalised with a bifunctional chemical group. Similar to the second reaction of part one, added trans-Cyclooctene-PEG4-NHS ester reacts with free amine groups, in the structure of the antibody, to form a stable amide. Primary amine (-$NH_2$) groups are mostly found in lysine (Lys) and arginine (Arg) residues of antibodies[43]. In this reaction, the abundance of antibodies relative to trans-Cyclooctene-PEG4-NHS necessitates maintaining a pH of 7.5 to ensure the stability of NHS. While doing so, the probability of $NH_2$ existing in its protonated form is considered acceptable. The reaction can be seen in Figure 7 below.

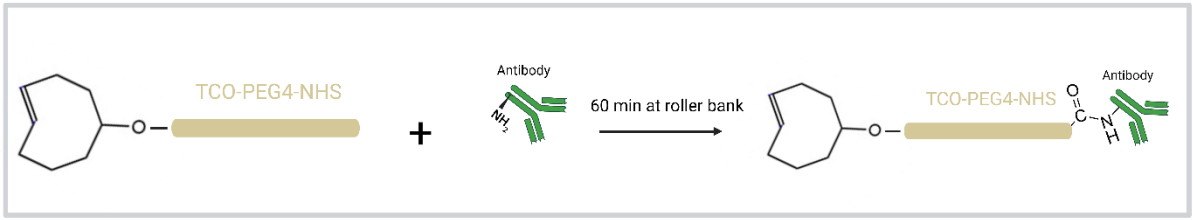


*Figure 7: Schematic representation of the reaction of TCO-PEG4-NHS reacting with free amine groups in the antibody structure, forming an amide bond. Reactants were incubated for 1 hour on a roller bank at neutral pH (image was made using Biorender).*

### 3.2.3 Capturing the HCC derived EVs

In the context of investigating the concept of the system, the objective is to maximize the presence of HCC derived EVs. To achieve this, HepG2 cells, a cell line derived from the tumour of a HCC patient, are cultured to the maximum confluency of between 90-100%. Subsequently, the cells are starved for 48h as research has suggested that cell starvation increases the production/excretion of EVs [44]. After starvation of the cells their conditioned medium is collected, cleaned from cells and debris, and concentrated with tangential flow filtration (TFF) to achieve the highest concentration of EVs possible. Additionally, research has shown that HepG2 cells do express both ASPGR1 and EpCAM [41].

When the sample with conditioned medium is concentrated the functionalised antibodies are used to capture EVs. This step completes the secondary elementary part of the system, which is visualised in Figure 8.

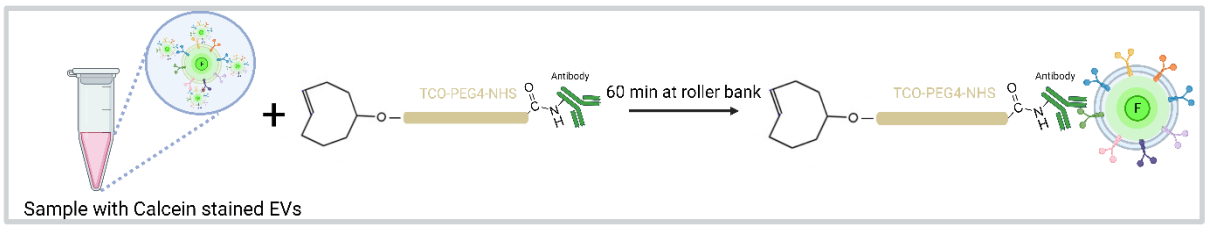


*Figure 8: Schematic representation of antibody-TCO conjugates capturing Calcein stained EVs from conditioned medium. Reactants were incubated for 1 hour on a roller bank at neutral pH The circle, with the letter F, indicates fluorescent activity of the Calcein in the FITC channel (ex 488 ; em 530/30) (image was made using Biorender).*

### 3.2.4 Conjugating the two elementary parts

The most important reaction in the assembly of the system is conjugating the earlier mentioned elementary parts. The “click” reaction between Tetrazine and trans-Cyclooctene (Figure 9), also called an inverse electron-demand Diels-Alder (iEDDA) reaction binds the magnetic beads to the antibody-EV construct. Without the need for a catalyst, this reaction is both rapid and specific, and also compatible with biological systems[45].

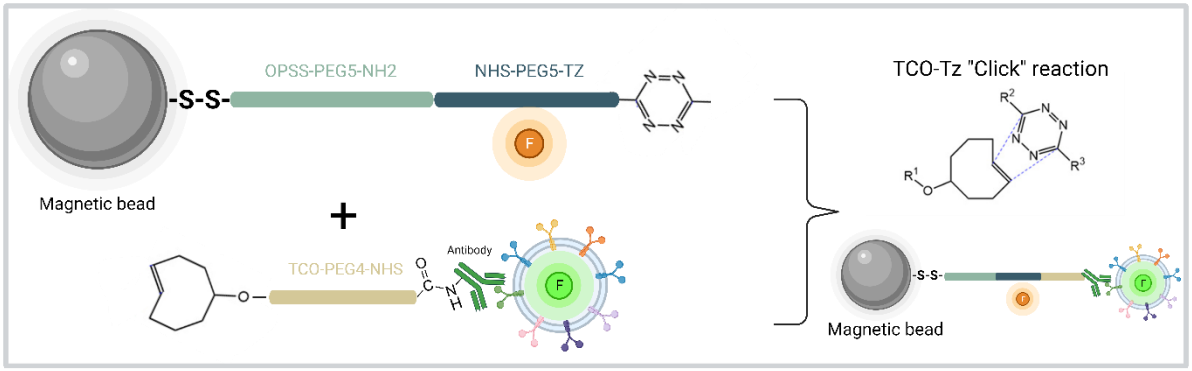


*Figure 9: Schematic representation of the “Click” reaction between the Tz functionalised magnetic beads and the TCO functionalised EVs (captured by antibodies). The reactants are incubated for 1 hour on the roller bank at neutral pH. The result of the reaction is the finalised capturing system with captured Calcein stained EVs. Circles, with the letter F, indicate fluorescent activity of the Tz group and the Calcein staining (image was made using Biorender).*

## 3.3 Performance tracking of the system

To analyse the performance of the capturing system as proposed, the system needs to be controllable during and after the assembly process. Firstly, EV characterisation techniques need to be used to make sure the right EVs are present in the starting (collected) samples. Secondly, a successful chemical conjugation of the system has to be confirmed. Lastly, the capture of EVS by the system should be validated. As such, the in-process controls used to identify possible failures in the EV isolation system include:

### 3.3.1 Cryogenic transmission electron microscopy (cryo-TEM)

To verify that the sample concentrated from HepG2 conditioned medium actually contains EVs, the samples are visualised under an electron microscope. Using transmission electron microscopy the size, morphology and composition of biological samples can be evaluated. Some studies have utilized conventional transmission electron microscopy (TEM) to investigate EVs from conditioned medium [46]. However, a major drawback of this approach is that it necessitates sample preparation steps and techniques involving dehydration, chemical fixation, and/or staining, which may introduce artifacts and potentially alter the morphology, integrity and/or size of the EVs [47]. In cryo-TEM, these dehydration and chemical fixation steps are not necessary, thereby preserving the original morphology and integrity of the sample. The reason that it is not necessary is because cryofixation, used in Cryo-TEM is a technique used to rapidly immobilize biological samples at extremely low temperatures to preserve its structural integrity [48].

### 3.3.2 Nanoparticle tracking analysis (NTA)

To get an estimation of the number of EVs inside the biological sample, nanoparticle tracking analysis (NTA) will be performed. NTA measures the size distribution and concentration of nanoparticles suspended in a liquid solution. The technique is based on the (random) Brownian motion of the particles, this motion is created by the nanoparticles colliding with molecules of the solution that they are dispersed in. Typically, NTA is used for particles with sizes ranging from 10 to 2000nm.

Furthermore, NTA is only able to measure particle concentrations 1-10*$10^8$ particles/mL, therefore highly concentrated samples should be diluted first before their size distribution and actual concentration can be determined [49].

### 3.3.3 Calcein-AM staining of EVs

The particles in the conditioned medium sample are (expected to be) too small to visualise under a normal confocal microscope. The diffraction-limited resolution of conventional confocal light microscopes, typically in the range of 200-300 nm, poses challenges when studying particles as small as EVs [50]. To enhance the contrast and selective imaging of the EVs, fluorescent labelling is used. There are multiple ways of fluorescent labelling possible to visualise EVs, such as lipid dyes that colour the membranes, dyes that colour the lumen or (membrane)protein reporters. Each of these techniques comes with advantages and disadvantages. The lipid dyes colour almost every EV, but also produce a lot of false-positive signals that can originate from proteins, nucleic acids, or other lipid structures present in the sample. On the contrary, the (membrane)protein reporters will label the EVs more specifically, based on their (contained) proteins [51]. However, as explained earlier, EVs are highly heterogeneous, thereby limiting the fluorescent signal to a certain subtype of EVs with specific proteins in their lumen or on their surface. In this research, a lumen dye called Calcein-AM will be used, as this is an intermediate between the highly specific protein dyes and the non-specific lipid dyes [16,51].

The subpopulation that will be fluorescent after the Calcein-AM staining will be of esterase-containing EVs. The existence of this specific subpopulation can be attributed to the phenomenon illustrated in Figure 10, where it is demonstrated that the activation of certain enzymes within the EVs, known as esterases, is essential for cleaving off the acetoxymethyl (AM) ester groups. While Calcein-AM is cell permeable and non-fluorescent, the Calcein without its cleaved groups is highly fluorescent and loses its permeability, essentially trapping the fluorescent Calcein inside the vesicles [52]. This also means that fluorescent signal only stays inside of intact vesicles which limits the binding to other fragments or biomolecules. A limitation of this labelling technique is that after staining the EVs should be handled with caution to prevent membrane rupture and leakage of fluorescent Calcein out of the EVs.

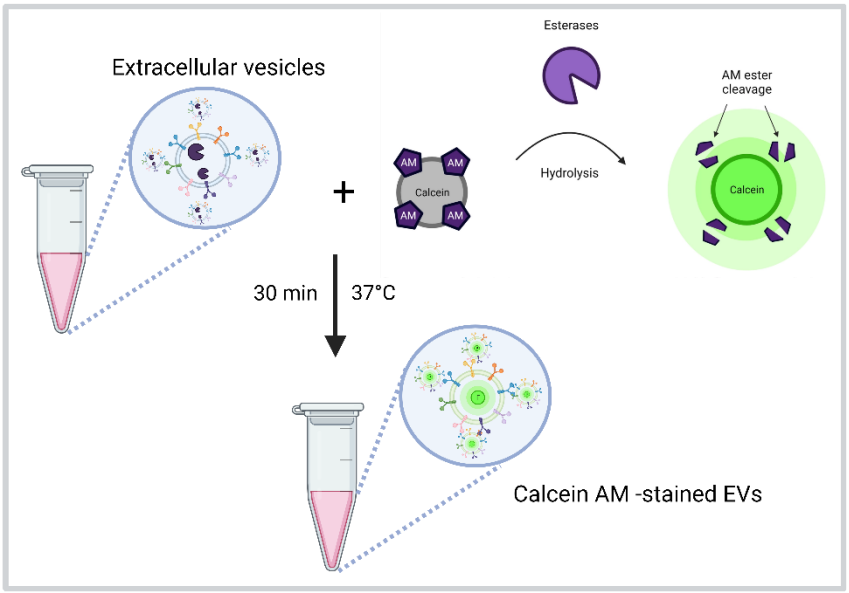


*Figure 10: Schematic representation of Calcein staining of the EVs. EVs were incubated with Calcein-AM for 30 minutes at 37°C. As soon as Calcein-AM enters the EVs, esterases hydrolyse the acetoxymethyl (AM) groups, releasing the fluorescent (in FITC channel) Calcein molecule (image was made using Biorender).*

### 3.3.4 Dot & Western blot

To verify that we start the procedure with a sample containing EVs, we need to evaluate the (surface) proteins on or inside the EVs. Combining the proteomic profile with the size, amount and morphology of the particles will provide sufficient information to conclude if the initial sample contains EVs.

Tetraspanins are a family of transmembrane proteins characterized by their distinct structure and conserved features. They are named "tetraspanins" because they typically possess four (tetra in Greek) transmembrane domains, which anchor them in the cell membrane. Tetraspanins are associated with the biogenesis, release, and uptake of EVs [53]. They participate in the sorting of proteins and lipids into EVs, influencing their cargo composition. Tetraspanins on the surface of EVs can also mediate interactions with target cells, facilitating EV uptake and modulating downstream cellular effects [53]. The defining characteristic of tetraspanins is their ability to form protein complexes known as tetraspanin-enriched microdomains (TEMs). These complexes are dynamic assemblies of tetraspanins and other transmembrane proteins, such as integrins, immunoglobulin superfamily members, and receptors [53]. As displayed in Figure 2, the tetraspanins CD9, CD63 and CD81 are known EV markers. CD9 will be evaluated in Dot & Western blot because of its abundance on EV membranes, consistent expression, established role in EV biology, availability of specific antibodies, and existing literature support [54–56].

Although presence of CD9 should confirm that the sample contains EVs, it does not provide any information about the origins of these EVs. Therefore, as mentioned in section 2.2.2, it is worthwhile to analyse the sample for the biomolecules EpCAM and ASGR1 as well.

Moreover, the proteins Calnexin and β-actin will also be evaluated by Western Blot. Calnexin is a type I integral membrane protein primarily located in the endoplasmic reticulum (ER), which is an organelle involved in the folding and processing of newly synthesized proteins. EVs are formed from plasma membrane invaginations or the ER and do not originate directly from the ER. Therefore, due to the distinct cellular localization of calnexin and the mechanisms involved in EV formation and cargo sorting, calnexin is expected to be absent or present at very low levels in EVs [57]. This allows calnexin to be a negative control protein in the Western Blot.

On the other hand, β-actin, also known as beta-actin, is a cytoskeletal protein that plays a fundamental role in the structure and function of cells. It is expressed in most cell types and is one of the six different isoforms of actin found in humans. β-actin is commonly used as a reference or housekeeping gene in Western Blot as its expression is relatively stable and consistent across different cell types and conditions [58]. This allows for protein normalisation and evaluation of reliability and reproducibility of the results.

### 3.3.5 Autofluorescence of Tetrazine

To evaluate the conjugation of the first elementary part of the system, Fluorescent activated cell sorting (FACS) (explained in more detail in the next subchapter), and microscopy can be used to evaluate the successful conjugation to Tetrazine due to the a typical reoccurring shift in the Pe channel (ex 488 ; em 585/40) (to higher fluorescence values). This phenomenon was described in earlier research done by the research group [59]. Furthermore, research [60] described Tz autofluorescence at λ=540nm, which would be visible in the Pe channel (ex 488 ; em 585/40) of both FACS and microscopy. To examine the effect of the conjugation the FACS gates are set based upon the empty beads (see Chapter 4.12).

### 3.3.6 Fluorescence activated cell sorting (FACS)

FACS combines flow cytometry and cell sorting capabilities. Flow cytometry involves the use of laser-based technology to analyse and quantify various characteristics of individual particles, such as size, granularity, and the presence of specific surface markers. Gates (filters) can be set based upon these characteristics. These gates can then be used to sort out the particles that fall within the gates, using electrostatic charge.

The capturing of Calcein stained EVs by the antibody functionalised magnetic beads, can be validated using FACS. By setting gates based on FITC (ex 488 ; em 550/30) channel positivity, the captured EVs can be detected based on a higher fluorescence value compared to empty beads. The gates for the Pe channel (ex 488 ; em 585/40) (used for validating Tz conjugation) and FITC channel (ex 488 ; em 550/30) are calibrated by making use of empty bead controls and fitting the gates around those populations. The gates can be seen in Chapter 4.12.

By using a different second gating strategy, all events that are positive in both the Pe channel (ex 488 ; em 585/40) as in the FITC channel (ex 488 ; em 550/30) are marked as being “double positive”. The criteria for being positive in the FITC channel (ex 488 ; em 550/30) and Pe channel (ex 488 ; em 585/40) slightly vary compared to the earlier used gating strategy. The reason for this change in strategy is to prevent the bulk of the “right shift” in the channels to fall just out of the gates, and see what effects it has on the results. The “double positive” gates can also be found in Chapter 4.12.

# 4. Materials and methods

## 4.1 Cell culture

The human HCC cell line HepG2 (ATCC, Virginia, United States) was used in this study. The cells were maintained in high glucose Dulbecco's modified Eagle Medium (DMEM, Lonza, Verviers, Belgium) supplemented with 10% fetal bovine serum (FBS, Lonza) and antibiotics ( 50U/ml Penicillin and 50 µg/ml streptomycin, Sigma, St. Louis, MO, USA). They were passaged twice a week when they reached nearly 100% confluency, using a 1:5 split ratio. The cells were detached from the culture plate using 0.05 % trypsin-EDTA, (Gibco, NY, USA) at 37°C for 5 minutes. The detached cells were resuspended in fresh medium and split at a ratio of 1:5. The incubator used in the experiments maintained conditions at 5% $CO_2$ and 37°C.

To starve the cells, the cells were grown to nearly 100% confluency in the normal culture medium (10% FBS). Then, the medium was removed and replaced with starvation medium (high glucose DMEM, 0% FBS, with antibiotics). The cells were incubated for 48 hours in a 5% $CO_2$ incubator at 37°C.

## 4.2 Collection of extracellular vesicles

The medium from HepG2 cells cultured in 175 $cm^2$ culture flasks was centrifuged at 300 x g for 10 minutes, followed by a second centrifugation at 2800 x g for 10 minutes. After each centrifugation step, the supernatant was collected. Supernatant was either directly concentrated using tangential flow filtration (TFF) and stored at 4°C for further experiments the same week, or stored at -80°C for further analysis at larger timeframes.

## 4.3 Tangential-flow filtration (TFF)

The TFF column (TFF-Easy-tangential flow filtration EV concentrator 1; HansaBioMed, Estonia) was set up according to the manufacturer's instructions. Briefly, the TFF column was primed before sample loading using a 10ml Luer-Lock syringe (Becton Dickinson, NJ, United States) filled with phosphate buffered saline (PBS). Thereafter, the sample of interest was loaded and concentrated up to 20 times using the TFF column. The concentrated EV sample (total approx. 1ml) was collected, temporarily stored at 4 °C, and the TFF column was washed with MilliQ. The TFF column can be re-used up to 25 times.

## 4.4 Nanoparticle tracking analysis (NTA)

The conditioned medium of a T175 (175 $cm^2$) cell culture flasks containing starved HepG2 cells (similar to 4.1) was collected (4.2) and was concentrated from 30ml to 1,5ml using TFF (4.3). The sample of EVs was diluted in PBS (1:50 or 1:100) to reach between 10-20 particles per frame. After dilution, a sample of minimal 500µl was loaded into the Nanosight NS500 (Malvern Instruments, Malvern, United Kingdom) and analysis was performed according to the manufacturer's instructions. Starvation medium was used as a negative control for the detection of background particles, not originating from EVs. Particle size distributions and concentration estimates were obtained using the accompanying software (NanoSight Software NTA 3.1, Malvern Instruments).

## 4.5 Cryogenic transmission electron microscopy (Cryo-TEM)

The conditioned medium of three T175 (175 $cm^2$) cell culture flasks which contained starved HepG2 cells, (similar to 4.1) was collected (4.2) and was concentrated from 90ml to 1,5ml using TFF (4.3). Cryo-TEM was used for direct visualization of vesicles. An aliquot (3 µL) of sample was deposited on glow-discharged holey carbon-coated grids (3.5/1 Quantifoil Micro Tools, Jena Bioscience, Germany). After the excess liquid was blotted, the grids were vitrified in liquid ethane using a Vitrobot (FEI, Eindhoven, The Netherlands) and transferred to a FEI Tecnai T20 electron microscope equipped with

a Gatan model 626 cryo-stage operating at 200 keV. Micrographs were recorded under low-dose conditions with a slow-scan CCD camera. The size of individual particles are quantified with NIH ImageJ software (NIH, Bethedesa, MD).

## 4.6 Dot-Blot

The conditioned medium of a T175 (175 $cm^2$) cell culture flasks which contained starved HepG2 cells, (similar to 4.1) was collected (4.2) and was concentrated from 30ml to 1,5ml using TFF (4.3). These samples were diluted in PBS at various ratios (1:0, 1:1, 1:2, 1:5). Five microliters (5µL) of each diluted sample was spotted onto a nitrocellulose membrane (GE healthcare life sciences, Upsala, Sweden) which was pre-cut into four pieces. The membrane pieces were then blocked with 5% non-fat milk (Bio-rad, CA, United States) in Tris-buffered saline with 0.01% Tween-20 (TBS-T) for 1 hour. Following the blocking step, the membranes were washed three times for 5 minutes each with TBS-T. Thereafter, the membranes were incubated with primary antibodies: CD9 (mouse monoclonal, 1mg/ml), EpCAM (rabbit monoclonal; 0,7mg/ml), and ASGR1 (rabbit polyclonal; 0,1mg/mL), for 1 hour at room temperature on a roller mixer. Subsequently, the membrane pieces were washed again three times for 5 minutes each with TBS-T. Next, the membrane pieces were incubated with secondary antibodies, goat anti-mouse for CD9 (polyclonal, 1mg/ml), goat anti-rabbit for EpCAM (polyclonal; 0,3mg/ml), and goat anti-rabbit for ASGR1 (polyclonal; 0,3mg/ml), for 1 hour at room temperature on a roller, followed by another round of washing. Lastly, the membrane pieces were incubated with a tertiary antibody, rabbit anti-goat (polyclonal; 0,55mg/ml) antibodies conjugated to horseradish peroxidase (HRP), for 1 hour at room temperature on a roller mixer, and washed again three times each with TBS-T. Membranes were visualized using enhanced chemiluminescence (ECL, Thermo Scientific, MA, United States). For additional information about antibodies, see supplementary Table 1.

## 4.7 Western blot

Protein samples obtained from cell lysates (controls) or samples obtained from TFF (conditioned and starvation medium) were sonicated for 10 seconds to denature their proteins. Subsequently, the samples were diluted (1:4) in loading buffer containing 4x Lamelli sample buffer with beta mercapthoethanol and denatured at 95°C for 5 minutes. 20 µl of the denatured samples, were loaded onto a 10% sodium dodecyl-sulfate polyacrylamide gel (SDS-PAGE) for electrophoresis. Electrophoresis was performed at a constant voltage of 90 V for 30 minutes and 120 V for 90 min until the samples reached the resolving gel. Following electrophoresis, proteins were transferred from the gel to a PVDF membrane (Sigma) by wet transfer. The membrane was then blocked with 5% non-fat dry milk in TBS-T for 1 hour at room temperature.

After blocking, the membrane was incubated overnight at 4°C with primary antibodies targeting ASGR1, EpCAM, CD9, Calnexin (monoclonal, 26µg/ml) and β-actin (AC-15 clone, NA) (See supplementary Table 1), diluted in blocking solution. Subsequently, the membrane was washed multiple times with TBS-T to remove unbound primary antibodies. Following the washes, the membrane was incubated with appropriate secondary antibodies conjugated to horseradish peroxidase (HRP) for 1 hour at room temperature. For Calnexin secondary antibody was goat anti-rabbit (polyclonal; 0,3mg/ml) and for β-actin it was goat anti-mouse (polyclonal; 1mg/ml).

Again, the membrane was washed thoroughly with TBS-T to remove unbound secondary antibodies. Protein bands were visualized using enhanced chemiluminescence (ECL, Thermo Scientific). The intensity of imaged protein bands were quantified using NIH ImageJ software (NIH, Bethedesa, MD, United States).

## 4.8 Calcein-AM staining

Staining solution (10µM Calcein-AM in PBS) was made with 1µL Calcein-AM (Invitrogen, 1mM) and 100µL PBS. To this 100µL of conditioned medium sample from TFF (4.3) was added. After adding the TFF samples, the resulting solution was incubated for 30 minutes in a water bath maintained at a temperature of 37°C. This incubation step was performed to facilitate the activation of esterase activity.

## 4.9 Fluorescence microscopy

Samples obtained after Calcein staining were evaluated using fluorescence microscopy (Nikon Eclipse Ti, Amersfoort, Netherlands). 10µL of the sample was pipetted into a cell counting slide and put under the microscope for examination. In a different experiment samples obtained after functionalisation of beads with Tz, were visualised under the microscope. As controls, OPSS conjugated beads were imaged. Samples were evaluated in brightfield, Pe and FITC channels. Scalebars indicating the magnification were made using NIH ImageJ software (NIH).

## 4.10 Conjugation of the system

The conjugation of the system, from magnetic beads to EVs, can be subdivided into three main conjugation reactions as also described in Chapter 3. First, beads are conjugated to Tetrazine then antibodies are conjugated to TCO. Lastly, the two products of the first reactions will be coupled together.

### 4.10.1 Functionalisation of beads with Tetrazine (TZ)

100µL of AccuBead™ Thiol Magnetic Beads (30mg/ml; size 1-5 µm; Bioneer, Daejeon, Republic Korea) were conjugated to 7.2µL of OPSS-PEG5-NH2 (dissolved in DMSO at 30mg/mL; Nanocs/Bio-connect, NY, United States) in 92.8µL PBS using a roller mixer at room temperature for 2 hours. The conjugated beads were then washed 5 times with PBS using a strong magnet, and resuspended in 100µL of PBS. Subsequently, 7.9µL of 6-methyl-tetrazine(TZ)-PEG5-NHS (dissolved in DMSO at 30mg/mL; Jena Bioscience) was added to 92.1µL of PBS (pH=8.5) and mixed with 100µL of the conjugated beads. The reaction was carried out at room temperature for 2 hours using a roller mixer. The beads were then washed 5 times with PBS and stored in 100µL of PBS with 1% BSA at 4°C and could remain stable this way for up to 4-8 weeks.

### 4.10.2 Conjugation of Antibody (EpCAM or ASPGR1) to TCO

TCO – PEG4 – NHS ester (3 mg/mL in DMSO, Jena Bioscience) was stored at -20°C. A 10 µg/mL antibody solution in 100 µL PBS was prepared. To the antibody solution, 8.6 µL TCO-PEG4-NHS and 91.4 µL PBS were added. The mixture was incubated on a roller mixer at room temperature for 1 hour. Purification was performed using Amicon ultra 0.5 mL filters (Darmstadt, Germany), with three repetitions of centrifugation (5000 rpm, 20 min) and resuspension in 100 µL PBS. The column was then spun in reverse (5000 rpm, 5 min) to obtain a 200 µL antibody-TCO solution. To ensure optimal use, this solution was prepared fresh and used immediately for further conjugation.

### 4.10.3 Coupling of the groups

Calcein-AM stained EVs were coupled with antibody-TCO. 50 µL of the EV sample was incubated with the antibody-TCO (10 µL) on a roller mixer for 1 hour, protected from light. Conjugated beads (5 µL) were then added and incubated for an additional hour. The solution was washed three times with PBS containing 1% BSA to remove unbound components. This coupling method allowed for specific labelling of EVs, enabling subsequent analysis and characterization. Proper controls were taken to make sure coupling method allowed for specific labelling of EVs, enabling subsequent analysis and characterization. After conjugation samples were analysed using FACS.

## 4.11 Release by Dithiothreitol (DTT)

Samples obtained after conjugation of the first elementary part of the system, Beads-OPSS-Tz, were resuspended in 100µL of PBS. A solution was made containing 50mM DTT (Sigma) in milli-Q , and 100µL was added to the Beads-OPSS-Tz. Beads were incubated for 5 minutes, 15 minutes, 30 minutes and 1 hour respectively. After incubation the beads were washed 3 times with PBS and analysed using FACS.

## 4.12 Fluorescence activated cell sorting (FACS)

Conjugated samples, together with appropriate controls, were diluted with PBS to a minimal volume of 300µL for sample tube loading. This to minimize chances of air getting into the FACS sorting machine (BD FACSaria II, San, Jose, California). Flowrate was set at 11. Sample agitation speed was between 100-300 rpm. Voltages were set as: FCS 200, SSC 280, Pe (ex. 488 ; em. 585/40) 400, FITC (ex. 488 ; em. 530/30) 400. Lens filter of 1,5 ND was used to acquire the events. Events were acquired until reaching 10.000 events or less (if 10.000 events was unreachable due to low events/sec).

Data analysis was performed accompanying software (BD FACSaria II) using the following gating strategies. Statistical analysis: All data is presented as mean ± standard error of the mean (SEM). Using unpaired students' t test, the differences were considered statistically significant at $p < 0.05$. (IBM SPSS Statistics 28.0, NY, United States)

First gating strategy (as explained in Chapter 3.3.6) is displayed in Figure 11.

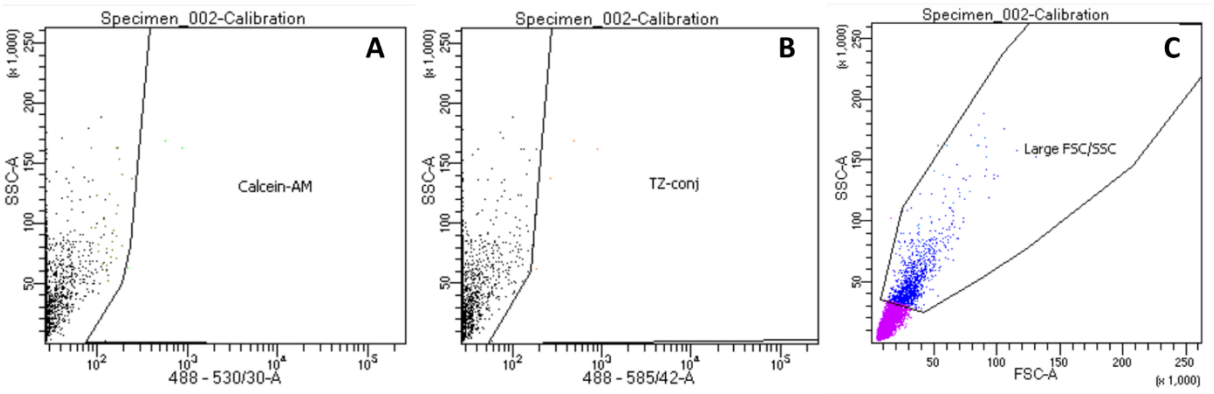


*Figure 11: The first gating strategy used for FACS data analysis. (A) Gate that indicates if measured events are positive in the FITC channel (ex 488 ; em 530/30). (B) Gate that indicates if measured events are positive in the Pe channel (ex. 488 ; em 585/50). (C) Gate that indicates if measured events have a high value for both forward scatter (FCS) as well as side scatter (SSC). Forwards scatter being indicative for size and side scatter for granularity.*

Second gating strategy (as explained in Chapter 3.3.6) is displayed in Figure 12.

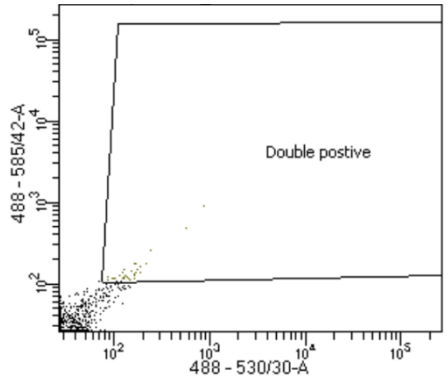


*Figure 12: Gate indicating events that are positive in both Pe channel (ex. 488 ; em 585/50) as well as FITC channel (ex 488 ; em 530/30). This gating strategy has slightly different values to determine what is marked as positive.*

# 5. Results & Discussion

## 5.1 Characterisation of extracellular vesicles

The EVs isolated from the HepG2 cell line were subjected to a series of experiments to confirm their identity and integrity. Their small size and heterogeneous nature present challenges for imaging and identification, particularly when it comes to determining their cellular origin. As a result, it can be difficult to confidently determine whether a given population of EVs is derived from a specific cell type, such as HepG2 cells. Another challenge arises from the fact that biological samples containing EVs are often contaminated with proteins, lipids, nucleic acids, and other cellular debris that are released into the extracellular space, which can interfere with the analysis and isolation of EVs [61]. Therefore the combined results of NTA, Cryo-TEM, Dot-Blot, Western-Blot, microscopy and FACS will be used to confirm the identity, sizes and origins of the EVs in this subchapter.

### 5.1.1 Nanoparticle tracking analysis

Nanoparticle tracking analysis (NTA) is performed in order to get an estimation of the amount of extracellular vesicles inside the biological sample of the conditioned HepG2 starvation medium. Furthermore NTA can provide insights on the particle size distribution of the sample, which could help (together with other results) to confirm that the particles measured are indeed EVs. Supplementary Figure 1, illustrates the size distribution plots for the analysed samples. The graphs consistently reveal a heterogeneous population of particles with varying sizes, yet none of them exhibit particles larger than 500 nm. These findings validate the success of the centrifugation protocol (prior to TFF) in effectively removing cells and other larger particles from the sample. The predominant size range of particles within the test samples falls between 50 nm and 300 nm, which is a typical size range for small EVs. However, no conclusive statements can be made regarding the origins of these particles as agglomerated proteins or lipids could fall into the same size range.

The average particle concentration in the EV samples, measured by NTA, was $(1{,}73 \pm 0{,}66) * 10^8$ particles per ml. Furthermore $0{,}95 * 10^8$ particles per ml, were measured in the medium control sample as can be seen in Figure 13. Unfortunately, no definitive conclusions can be drawn regarding the concentration of EVs. This limitation arises from the insufficient disparity in total particle counts between the control medium and conditioned medium, which hinders any assumptions.

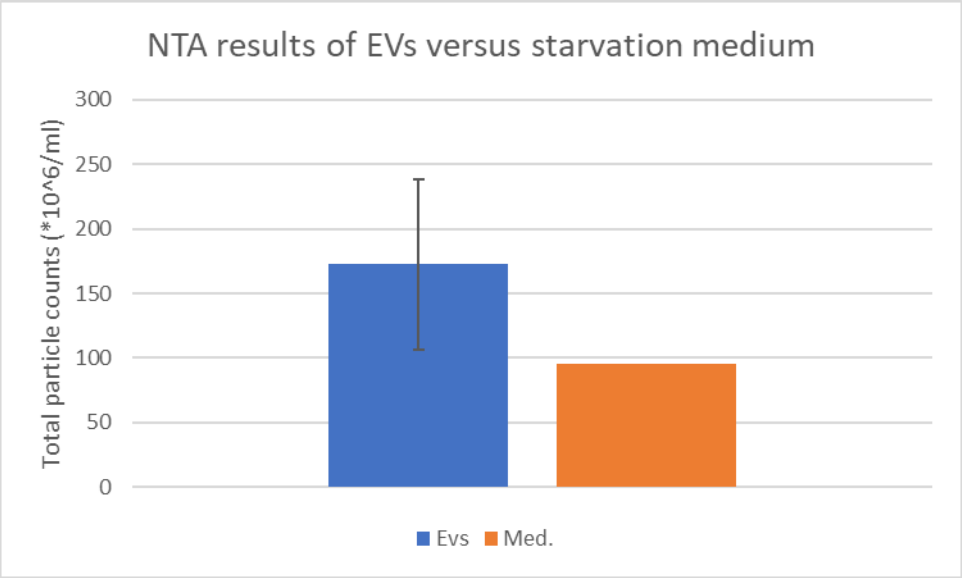


*Figure 13: Comparison by NTA particle counts of conditioned medium (expected to contain EVs; depicted as EVs) and starvation control medium (depicted as Med.). The average particle concentration in the EV samples, measured by NTA, was (173±66)*$10^6$ particles per ml.*

Furthermore, due to the recovery of only one of the control medium measurements, it is not feasible to subject it to statistical analyses. The phenomenon of particle counts in the medium being higher than expected, which was visible in the NTA results more than once (also in lost data), could be explained by the procedure for concentrating the particles. Firstly, the TFF column used to concentrate the samples (and also the control medium) is used more than once. Therefore, although it was properly washed whenever it was used, there could be residual particles from earlier run experiments present in the column that might have influenced the NTA particle reading. Secondly, and this holds for both controls as for measured samples, the samples could be contaminated by silicone oil nanoparticles. During the concentration with TFF, the samples are pumped in and out of the column using BD 1ml Luer-lock syringes. To enable smooth gliding of the plunger, these syringes contain a small lubrication coating of silicone oil on the inside which might come loose after resuspending several times. Research has shown that these silicone nanoparticles can contaminate samples inside the syringes, most noticeable when injection ophthalmic drug solutions [62]. However no paper could be found containing data on particle concentrations with sizes 50-300nm based on NTA.

### 5.1.2 Cryo-TEM

Using cryogenic transmission electron microscopy (Cryo-TEM) the size, morphology and composition of biological samples can be evaluated. Thereby enabling visual confirmation or denial that the initial sample contains EVs. The Cryo-TEM measurements showed clusters (Figure 14a) or singular (Figure 14b) bilayer structures ranging in the sizes from 100nm to 300nm. Unfortunately there were not enough pictures containing EVs to make a conclusive verdict on a general size or morphology. However, Figure 14a and Figure 14b depict EVs with round morphology with a singular lipid bilayer. Besides the lipid bilayer structures, there are a lot of electron dense regions that are not bilayer structures. The observed artifacts, highlighted in red (figure 14a), are most likely originating from amorphous ice contamination. This hypothesis is supported by the irregular clumps/clusters lacking clear definition and structure, similar to death cells under a microscope, which is typical for these type of contaminations [63].

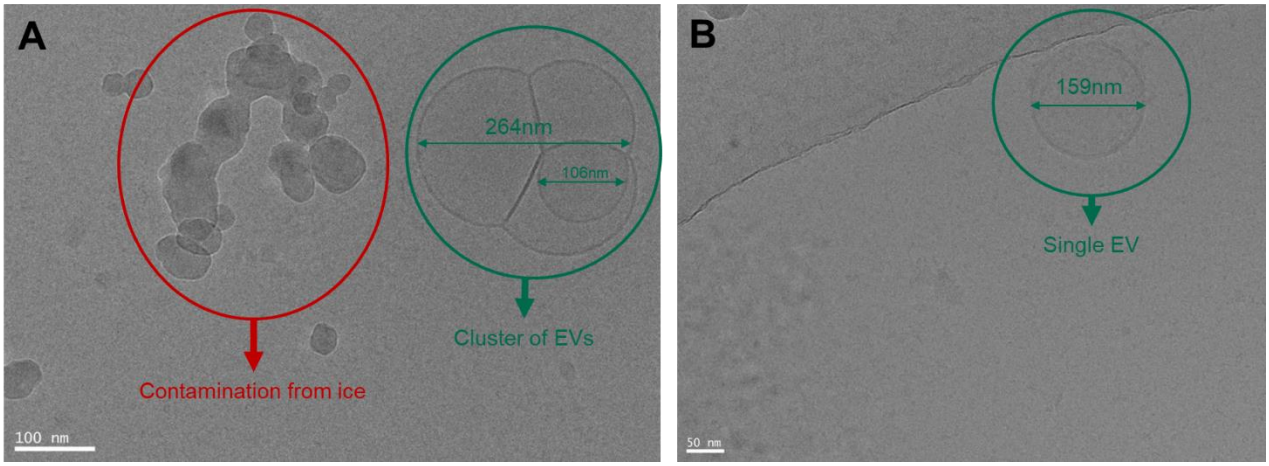


*Figure 14: Cryo-TEM pictures made displaying EV morphology with scalebars (bottom left). (A) In the green circle a cluster of EVs is identified having a total diameter of 264nm, with the smallest EV of the cluster having a diameter of 106nm. In red an electron dense region is highlighted that probably originates from ice contamination. (B) A single EV is shown with a lipid bilayer structure and a diameter of 159nm.*

### 5.1.3 Dot blot

Dot blot is performed to obtain insights into the concentration dependent profile of several proteins in the sample. This information functions as a piece of a puzzle that will ultimately determine if the particles in the sample can be confirmed to be EVs. In this subchapter, the findings from multiple Dot-Blot experiments conducted during the course of this research will be presented. Unfortunately, none of these experiments yielded outcomes that were in line with initial expectations. The subchapter will focus on discussing the most promising results obtained and their inherent limitations. Furthermore, it will outline the valuable insights gained from the "unsuccessful" Dot-Blot experiments.

In figure 15, Dot blot membranes are presented containing three conditioned medium samples and one starvation medium control each. Each dot in the Dot-Blot represents a specific measurement, as the samples are spotted in different concentrations. The intensity of the dots correspond to the amount of proteins EpCAM, ASGR1 and CD9 present. The results show that EpCAM, ASGR1 and CD9 are present in the conditioned medium samples.

When examining the results in Figure 15 in more detail, two things stand out. The first being the inverted spots on the membranes for the antibodies EpCAM and ASGR1. Excessive protein and/or antibody quantities typically result in the appearance of white dots in Dot-Blot (just like in Western-Blot [64]). This phenomenon occurs because when the chemiluminescence buffer is added, the substrate at that specific location is rapidly consumed. Consequently, during image capture, a void or complete absence of signal is observed at that particular spot. The second remarkable result is the positive signal in the starvation medium control. Reasons for it could be the TFF procedure, for the same reasons already mentioned in the NTA results (remaining particles in the column). Another explanation could be that something is present in the medium that non-specifically binds to the antibodies causing it to appear positive. When there is non-specific binding, it should be noted that this is limited to the primary antibodies as the control containing only secondary and tertiary antibodies did not appear to be chemiluminescent (supplementary Figure 2). Lastly, it is strange that in CD9, all three EV samples were positive when only PBS was spotted. A possible explanation could be that there has been a pipetting mistake. A positive remark on the results is the gradual decrease with concentration that is visible in most of the Dot blots. The strange “busted” dot in the $EV_{n=3}$

column of the CD9 blot is because of incorrect use of the tweezers to grab the blot and put it into the chemiluminescence machine.

Lessons learned from the Dot-Blot experiments include the fact that blocking the membranes with 5% BSA in TBS-T is insufficient. After blocking, the negative control with only secondary and tertiary antibody showed chemiluminescent signal, indicating unsuccessful blocking of the membrane. Another lesson learned is that removing the tertiary antibody decreases chemiluminescent activity. Removal of the tertiary antibody was intended to counteract the overexpression of chemiluminescence in the EpCAM and ASGR1 Dot blots. However, removing the tertiary antibody completely diminished the chemiluminescence activity from the membranes.

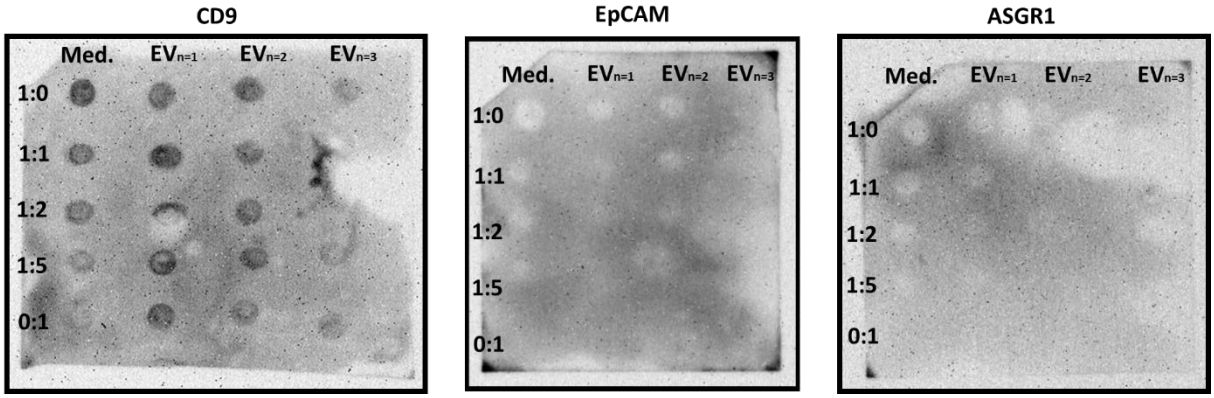


*Figure 15: Dot blots for a serial dilution of EV sample and starvation medium control for proteins CD9, EpCAM and ASGR1. White spots in the EpCAM and ASGR1 plot indicate overexpression of proteins. The "busted" dot in $EV_{n=3}$ at dilution 1:1 is caused by improper handling of tweezers to transport the membrane.*

### 5.1.4 Western Blot

Western Blot is performed, similar to Dot-Blot, to obtain insights into several proteins in the sample. While Dot-Blot produces primarily qualitative outcomes Western-Blot provides more quantitative information by enabling protein size determination. However, because Dot-Blot is quicker and easier it provides a better solution for measuring samples at multiple different concentrations.

The results of the Western Blot are partially displayed in Figure 16. Here, we blotted conditioned medium (expected to contain EVs), starvation medium (Med. in Figure 16) and HepG2 cells (Cells). These samples were evaluated for their expression of EpCAM, CD9, ASGR1, Calnexin and β-actin. In the figure only the results of CD9, ASGR1 and β-actin are presented this is because the EpCAM and Calnexin expression was too low to be detected, or absent (supplementary Figure 3).

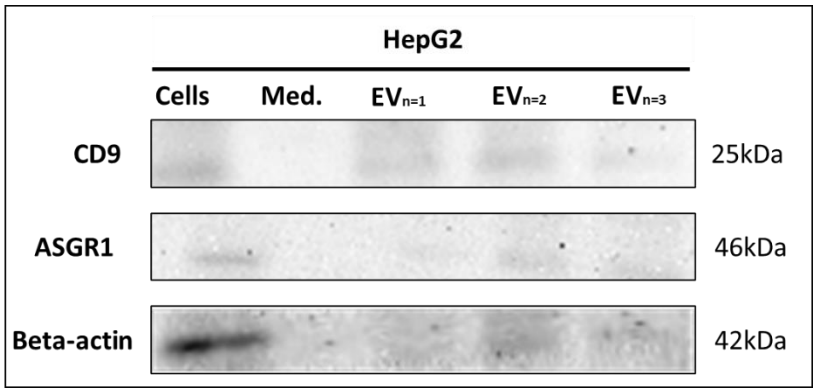


*Figure 16: Western blot results of proteins CD9, ASGR1 and β-actin. Proteins were measured for cell lysates (Cells), starvation medium control (Med.) and three EV samples.*

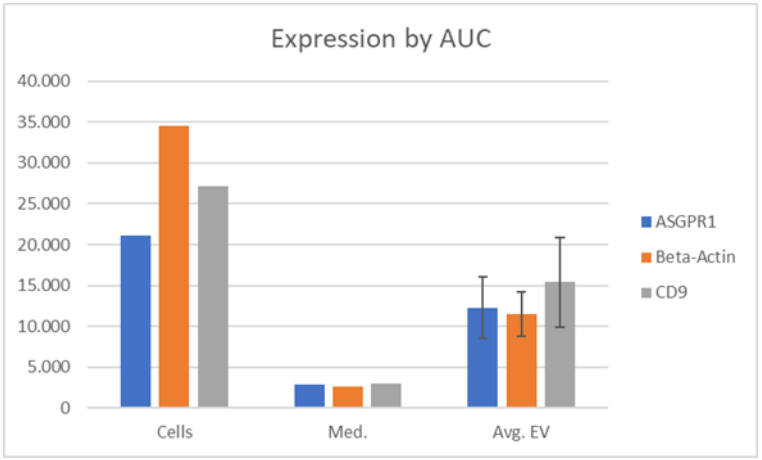


*Figure 17: Western blot data quantified using ImageJ and measurement of area under the intensity curves (AUC).*

When evaluating the plotted results in Figure 17, it can be observed that the expression of ASGR1, CD9 and β-actin is present in both cells and conditioned medium but absent in the control (starvation) medium. However it should be noted that for the cells and medium the experiment is only performed with one repetition. Quantifying the data involves measuring the area under the curve of the pixels in the picture, yielding the results depicted in Figure 17. The quantification of the pictures confirms the observations of the pictures, although again it has to be noted that these result are not statistically significant.

Calnexin is expressed in the ER and was used as a positive control for the cells. It was expected that Calnexin would be absent in EVs because of their lack of an ER system. The absence of the Calnexin in the cells can be explained by the protocol that was used during the Western Blot, as the Radioimmunoprecipitation assay buffer (RIPA) buffer was not used. Usually in Western Blot RIPA buffer is added to cells to disrupt the cell membrane, solubilize lipids, and create the necessary environment to maintain protein stability, preserve their native conformation, and prevent protein degradation during the lysis process. As we did not use RIPA buffer, the cellular membranes might have stayed intact or the proteins were not solubilized enough. The low EpCAM expression is unexpected when looking at the literature [7,41,65]. One possible explanation could be that the EpCAM expression is relatively low or that this particular type of antibody has lower affinity for EpCAM or is not very active (any more). Further research using different types of EpCAM antibodies could be helpful in the future.

The complete set of Western-Blot results, including the uncropped blots, Calnexin and EpCAM expressions, are provided in supplementary Figure 3. Analysis of these blots confirms the notable findings regarding the empty Calnexin and low EPCAM expression, as well as significant non-specific binding observed in the CD9, β-actin, and ASGR1 blots.

In the blot of CD9, a clear and highly expressed non-specific band can be seen at 90kDa in the three EV samples while being absent in the cells. The band is also lightly present in the starvation medium. Furthermore, multiple lighter non-specific bands can be seen above 30kDa. As explained in Chapter 2.4.3, CD9 is a protein from the Tetraspanins family and tends to form complexes called tetraspanin-enriched microdomains (TEMs). The TEMs can consist of heterodimerized or trimerized proteins consisting of CD9 and proteins involved with functions relating to endosomal/EV trafficking, multivesicular body (MVB) formation, or EV biogenesis [53]. The CD9 proteins can heterodimerize or trimerize (or even more) with these proteins and these complexes could be incorrectly stained by the CD9 antibodies in the Western blot. A potential protein that forms complexes with CD9 is ALG-2-interacting protein X (Alix)(90-100kDa), as reported previously [66]. Alix is known to be abundantly

present in extracellular vesicles (EVs) and is also found in cells, predominantly in their intracellular domain [67]. The absence of Alix signal in the cells may be attributed to inadequate cell lysis during the Western blot protocol. On the contrary, this would not explain the positively chemiluminescent band in the medium control. Bear in mind that the aforementioned explanations are purely speculative and should be considered as a hypotheses. Further research is required to validate these hypotheses and provide definitive confirmation. Other possible proteins responsible for the non-specific bands could be (combinations of) other tetraspanins such as CD63 (30-60 kDa) and CD81(26 kDa) or proteins affiliated to the endosomal sorting complexes required for transport (ESCRT) machinery [68]. CD63 has shown to be a protein with a very wide band in Western blot, further motivating the hypothesis [69].

While the level of non-specific binding in the ASGR1 blot is lower compared to that of CD9, it is still noteworthy and demands discussion. Analysis revealed non-specific binding in the 20-25 kDa range, leading to an exploration of small heat shock proteins (sHSPs) as potential cause [70]. sHSPs, including Hsp27 and Hsp20, are known molecular chaperones involved in cellular stress responses. They play essential roles in maintaining protein stability and preventing aggregation during stressful conditions. Considering their upregulation during nutrient deprivation [71], it was hypothesized that sHSPs might be present in EVs derived from starved cells, contributing to the observed non-specific binding. An alternative hypothesis could be that the bands are caused by cross-reactivity with small cytoskeletal proteins such as Cofilin [72].

β-actin exhibited the most distinct and prominent band among all cellular proteins in both the three EV samples as well as in the control group with cell lysate. When comparing this with literature, it is important to note that the detection of β-actin in EVs is not always consistent across studies, some studies have reported minimal or undetectable levels of β-actin in EV preparations [40,41] while others report similar β-actin levels to cell controls [42–44]. Although the expression of β-actin was positive for the cell control, it was lower than expected, as it is being recognized as a Western-Blot marker used for normalizing protein loading on the blot. The lower expression could, again, be explained by the fact that the cells might not have been fully lysed as β-actin is a cytoplasmic protein. Non-specific binding of the β-actin blot was comparable to the ASGR1 blot. The blot showed similar non-specific binding at low sizes around 20-25 kDa range and the higher non-specific band at 135-180kDa. Both bands exhibited greater expression in the EV samples compared to the cell controls, similar to the observations made in the ASGR1 blot. However, it should be mentioned that the nonspecific band corresponding to the larger proteins (135-180kDa) was far more intense in the β-actin blot compared to the ASGR1 blot. Reasons for the existence of these non-specific bands (other than for the same reasons as mentioned in the ASGR1 blots) are hard to determine as research has found different outcomes on β-actin expression in EVs, as mentioned earlier. Further experiments are necessary to confirm or deny the hypotheses and identify the specific proteins responsible for the non-specific binding.

### 5.1.5 Calcein staining of EVs

In order to confirm that the EVs can be stained with Calcein and become fluorescent, microscopy images are taken and EVs were run through FACS. The results of both of these techniques are visualised in Figure 18, both confirming successful Calcein staining. The FACS results show a clear shift in the FITC channel after Calcein staining, the addition of TCO-EpCAM did not seem to influence this shift. Before staining, only 5,8% (without TCO-EpCAM) and 6,0% (with TCO-EpCAM) of the measured events was positive in the FITC channel. After staining with Calcein these were 90,4% (without TCO-EpCAM) and 86,2% (with TCO-EpCAM) respectfully. It should be noted that the experiment was only caried out with a single repetition. However, Calcein stained EVs were taken as a control for different experiments and showed an average FITC positivity of 86,1% ± 6,2 (n=9), supporting the evidence found in this experiment. It is important to highlight that not all EVs are visible under the flow cytometer due to their small size, the actual percentage of Calcein stained particles (EVs) could therefore be different from the number displayed in the FACS plots. It might even be that all measured FACS events are clusters of EVs, allowing FACS imaging due to their relatively larger size. In accordance with the FACS results, the microscopy showed clear bright fluorescent spots (marked by the green circles) in the FITC channel.

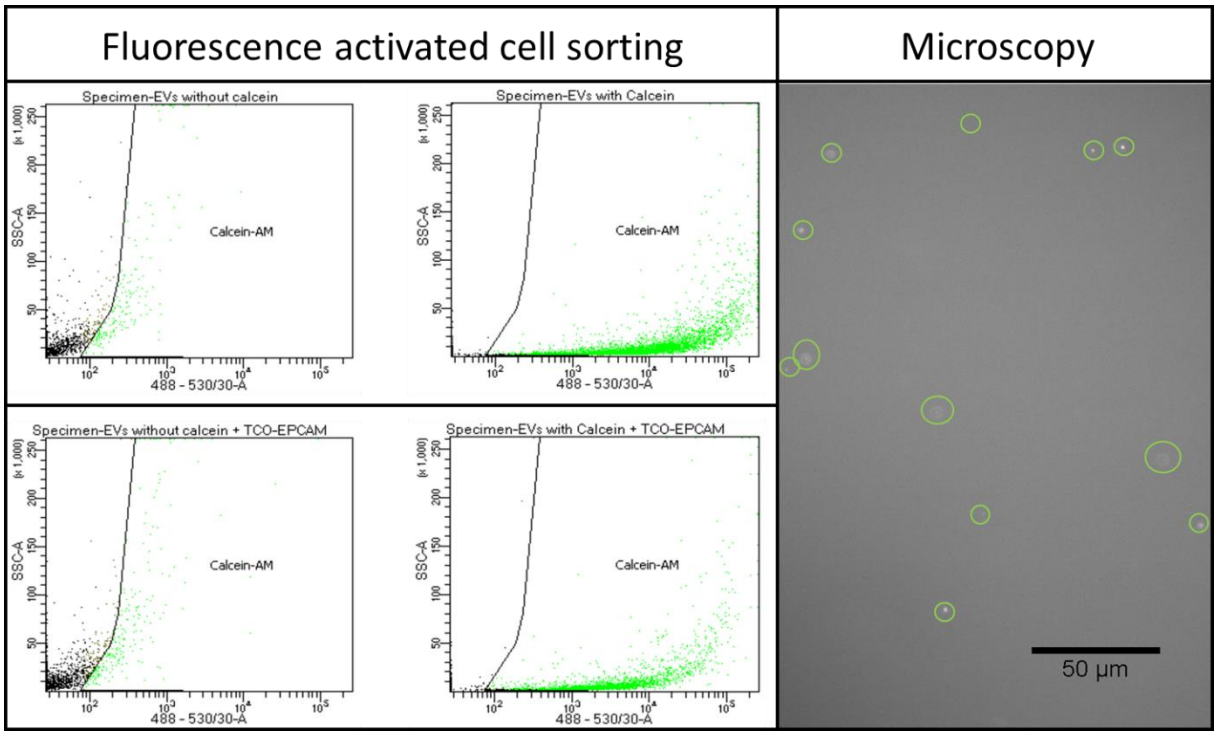


*Figure 18: Results of the Calcein staining of the EVs confirmed both by microscopy and FACS. FACS: (top pictures) Comparison between EVs with and without Calcein staining. (bottom) Same comparison, only the EVs are conjugated to TCO-EpCAM. Microscopy: Green circles indicate Calcein stained EVs in the FITC channel of the microscope (scalebar 50µm).*

## 5.2 Conjugation of the system

In the following chapter the results of the conjugation of the capturing system will be shown. The results of the chemical conjugation of magnetic beads to its Tz group will be discussed first. Thereafter the results will be shown of the full system including the capture of Calcein stained EVs. These results will primarily oriented around FACS data with the exception of one microscopy result for the intermediate Tz-beads.

### 5.2.1 The first elementary part of the system (Beads-TZ)

In this subchapter the results of the conjugation of the first elementary part of the system will be evaluated. Figure 6 in Chapter 3.2.1 displays how this particular part of the system should look like after conjugation (theoretically). The results on the successful functionalisation of magnetic beads with Tz are a combination of acquired data from both microscopy and FACS techniques. When looking at Figure 19, magnetic beads conjugated to OPSS can be seen in the brightfield channel (A) or in the Pe channel (ex 488 ; em 585/40) (B). Furthermore magnetic beads conjugated to Tz, also referred to as the first elementary part of the system, can be seen in the brightfield channel (C) or in the Pe channel (ex 488 ; em 585/40) (D). A general remark when looking at these pictures is that in some occasions smaller beads/particles stick to the larger beads, creating little clusters. These clusters seem to be more dense and might contain some unwanted adhered particles (dark black in A and C). When we compare the two types of beads in the Pe channel (ex 488 ; em 585/40) (B and D) we clearly see that the TZ-conjugated beads are auto-fluorescent in the Pe channel (ex 488 ; em 585/40) (D), while the OPSS-conjugated beads are not. Secondary to this observation it can be seen that a large portion of the PE positive beads are adhered to one or more (smaller) beads. An explanation for this phenomenon could be that the larger beads/clusters have a larger surface area making conjugation easier. Alternatively, the addition of Tz groups to the magnetic beads could alter their surface charge, since Tz groups are not easily ionizable while thiol groups are [36,73]. The altered surface charge could make the magnetic beads more susceptible to agglomeration or non-specific binding to contaminants.

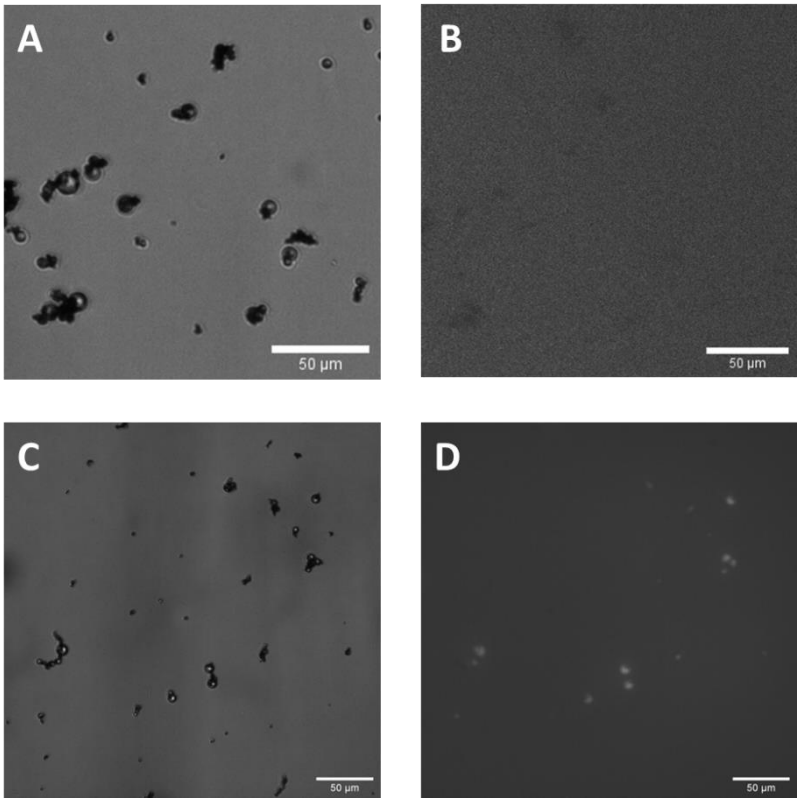


*Figure 19: Microscopy results of conjugation of first elementary reaction. (A) OPSS conjugated beads in brightfield. (B) OPSS conjugated beads in Pe channel. (C) Tz conjugated beads in brightfield. (D) Tz conjugated beads in Pe channel. Bright spots indicating successful conjugation to Tz.*

Figure 20 shows the FACS plots of naked beads (A), beads-opss (B), and beads Tz (C), where the side scatter was plotted against the Pe channel (ex 488 ; em 585/40). A clear right-shift in the Pe channel can be observed after the beads are conjugated to Tz (Figure 20c). Worth mentioning is that the gating strategy does not provide a clearcut yes or no answer about the Tz conjugation of a single bead, but can provide insights on the overall conjugation success. In the experiment displayed in the figure, the PE positivity of the sample jumped from 0.2% in empty beads, also named “naked beads”, (0.1% in OPSS-beads) to 19.9% after conjugation with TZ. Table 4, provides datapoints from multiple different repetitions of this part of the conjugation reaction. The datapoints show that, after testing, the increase in PE positive signal is statistically significant ($p<0,05$).

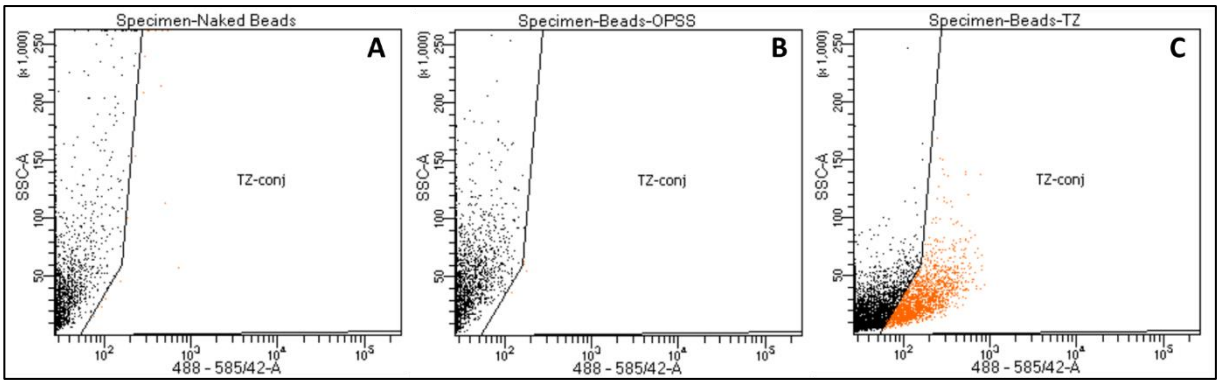


*Figure 20: FACS results of conjugation of first elementary reaction. (A) Empty beads negative in the Pe channel. (B) OPSS conjugated beads negative in the Pe channel. (C) Tz conjugated beads (partially) positive in the Pe channel indicating successful conjugation.*

From the aforementioned results in microscopy, it was hypothesized that a large percentage of agglomerated beads would be positive in the Pe channel and that this percentage would be higher than the percentage of Pe positive (small) single beads. To test the hypothesis, the gating strategy of high forward/side (f/s) scatter was applied to the experiments (as mentioned in Chapter 4.11). These results were also incorporated in Table 4. The results confirm the hypothesis that the percentage of beads that is positive for Pe is higher for the beads gated for having higher forward and side scatter, which is related to their size and granularity.

*Table 4: Percentages of Tz conjugation based on Pe channel positivity. Comparing empty beads, OPSS conjugated beads and Tz conjugated beads. The effect of high f/s scattering beads compared to low f/s scattering beads is also compared between the groups.*

| | **Empty beads (n=4)** | **Beads-OPSS (n=3)** | **Beads-Tz (n=4)** |
|---|---|---|---|
| **TZ-Conjugation (overall)** | 0,23%±0,13 | 0,13%±0,15 | 25,45%±4,29 |
| **TZ-Conjugation (low f/s scatter)** | 0,03%±0,05 | 0,00%±0,00 | 18,15%±2,74 |
| **TZ-Conjugation (high f/s scatter)** | 0,73%±0,48 | 0,53%±0,76 | 56,88%±5,73 |

During FACS measurements, it was observed that the Pe positivity of Tz-conjugated beads increased over time. In combination with previous results, a hypothesis arose that stated that the bigger (and thus heavier) agglomerates (which were more often positive for Pe) sank quicker to the bottom of the tube than small particles, thereby increasing the percentage of Pe positive beads. To test this hypothesis a test was set-up measuring the Tz conjugation immediately after vortex mixing or waiting for 60 seconds after vortex mixing and then acquiring the FACS data. The data is displayed in Figure 21.

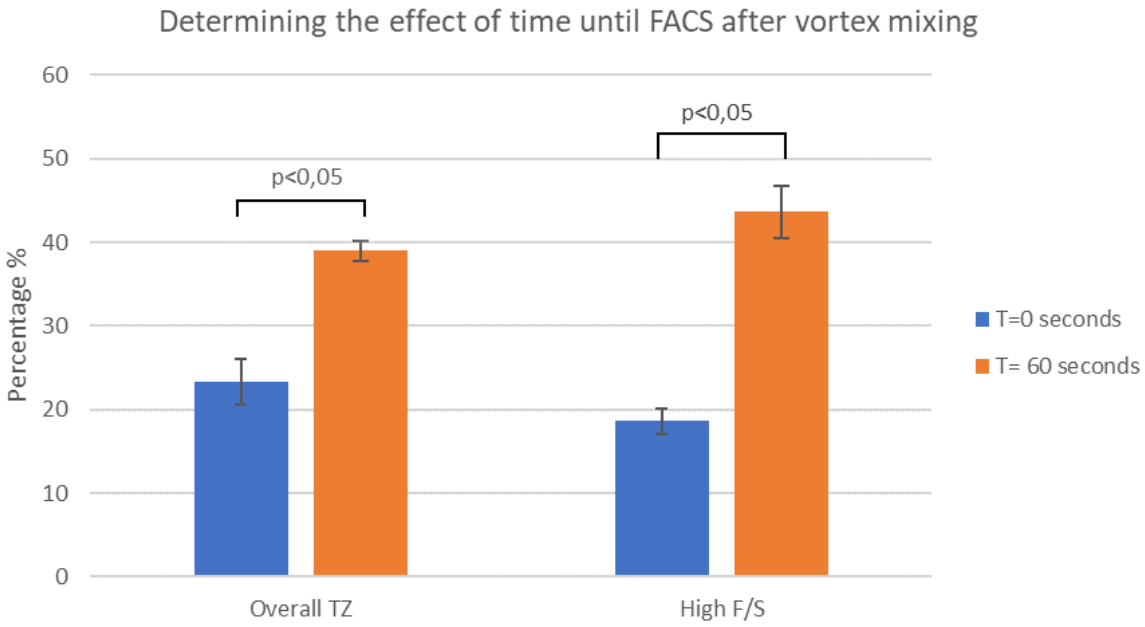


*Figure 21: The results for determining the effect of time waited after vortex mixing before FACS acquisition was started. T=0 seconds indicates beads that were immediately measured after FACS loading. T=60 seconds indicated beads that were measured after waiting 60 seconds. Data showed for T=0 seconds, an average of 23,3±2,77% Tz conjugation and 18,6±1,56% High F/S scatter. Data showed for T=60 seconds, an average of 38,97±1,25% Tz conjugation and 43,67±3,14% High F/S scatter.*

The data shows a significant (P<0,05; n=3) difference between slow measured beads (t=60s) and fast measured beads (t=0s) in both their Tz positivity, and their high forward/side scatter particles. Both these percentages are significantly higher for the t=60sec measured beads compared to the t=0sec measured beads. Next to this, the results were in accordance with the earlier found results that particles with high forward/side scatter have a higher percentage of positive particles in the PE channel after conjugation (not imaged in the figure). These results support the earlier formulated hypothesis that when the sample is running in the FACS machine, the bigger and heavier particles sink more quickly resulting in an increase of the percentage of Pe positive particles over time. However, this will eventually reach a plateau or decrease again when the smaller particles are sinking as well.

### 5.2.2 The full system with EVs (Beads-EVs)

After successful conjugation of the elementary parts of the system, the complete system can be conjugated. Results are gathered for both the full system with the EpCAM antibody as with the ASGR1 antibody. When EVs are captured by magnetic beads, a positive signal for both Pe and FITC is expected. To visualise the FACS results two types of gating strategies will be used, one will be focussed on the FITC and Pe channel separately while the other strategy will indicate “double positive” signals that are positive in both channels. The cut-off values of these strategies differ slightly, as explained in Chapter 4.12.

The FACS results show an increase in FITC positive signal after we conjugated the magnetic beads to the EVs. It should be noted however that error bars are high as it seems that two repetitions went as planned but one did not. In Figure 22, the shift in Calcein staining is displayed for all of the conjugated repetitions with the ASGR1 antibody. In the case of a successful conjugation (for instance the bottom left n=1 plot) the beads jump from 0,1% (empty beads) or 0,0% (Beads-TZ) to being 22,5% positive in the FITC channel, indicating the presence of fluorescein Calcein.

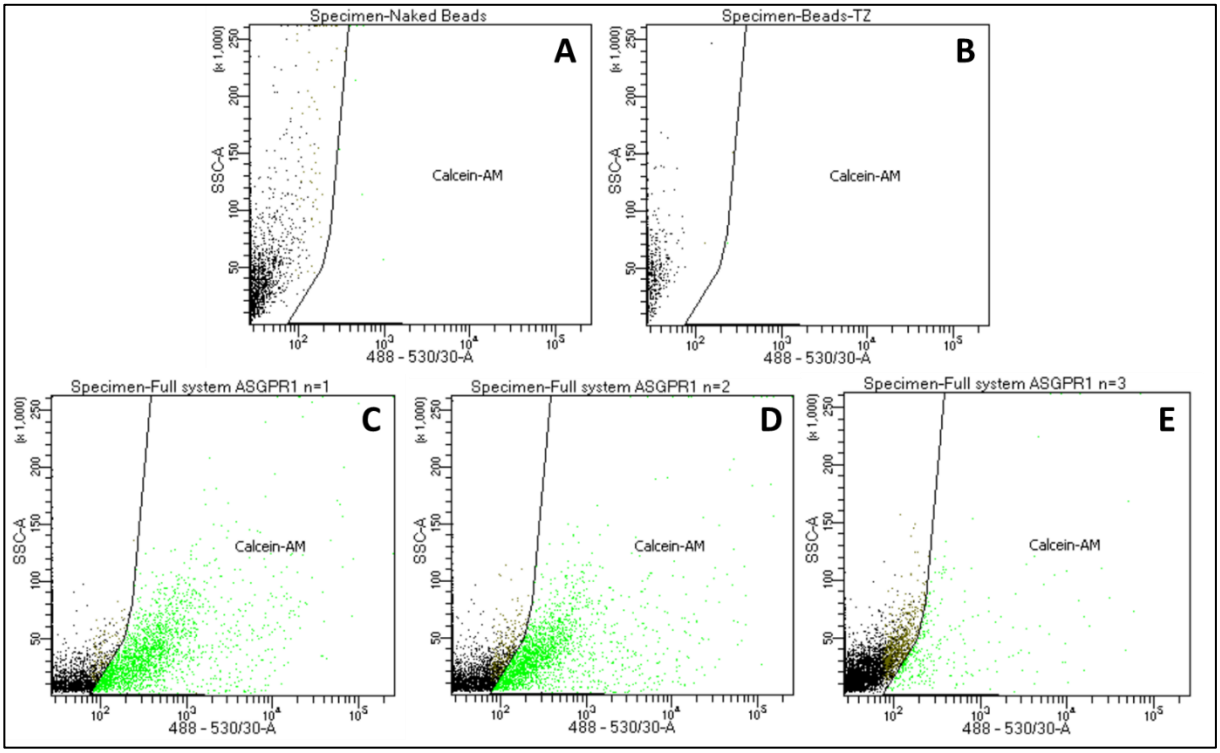


*Figure 22: Results of capturing system with antibody ASGR1 and Calcein stained EVs. (A) Empty beads being negative in the FITC channel. (B) Tz conjugated beads being negative in the FITC channel. (C & D) Successfully conjugated system displaying a clear right shift in the FITC channel, indicating capture of Calcein stained EVs. (D) Conjugated system with a right shift that is smaller than in C and D, indicating that only a small fraction of beads captured Calcein stained EVs.*

When comparing the full system with ASGR1 to the full system with EpCAM, as visible in Figure 23, it can be seen that there is no significant difference (P>0,05) between the two. Furthermore the average Tz conjugations of the systems for both ASGR1 and EpCAM conjugated beads, lie between 20-25%, which is similar to the Tz-conjugated beads and conform expectations.

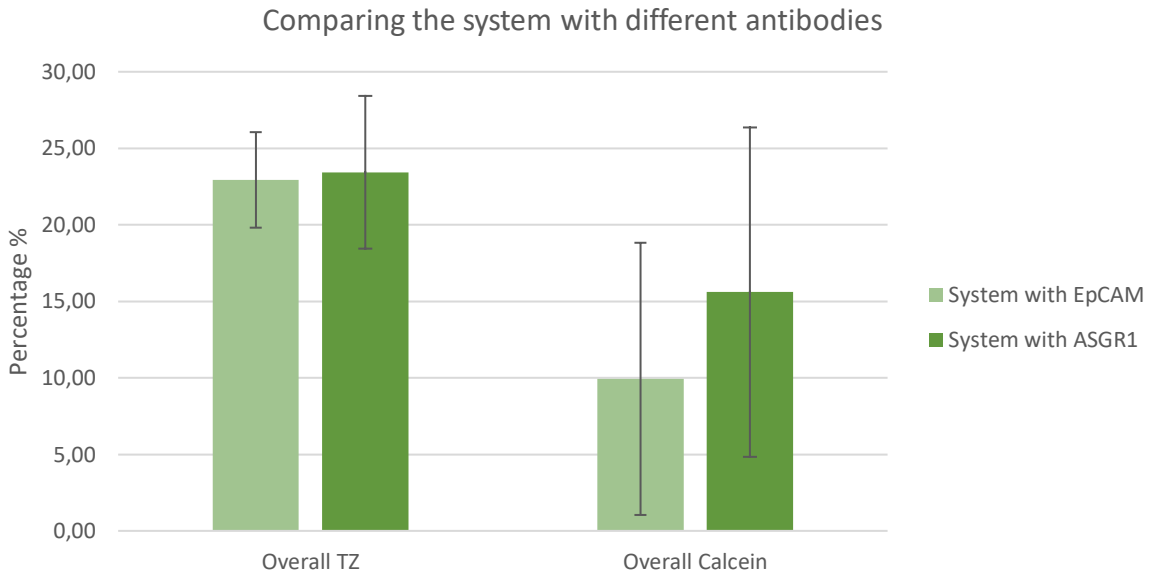


*Figure 23: Comparing the percentage of beads conjugated to Tz and Calcein stained EVs between systems with different antibodies (ASGR1 or EpCAM). The figure shows that there is no significant difference (p>0,05) between the two antibodies based on these results.*

The detailed version of the main results are displayed in Table 5, in which a comparison is made between the empty (or "naked") beads, beads conjugated to TZ and the two full systems with EpCAM and ASGR1 respectively. First, we observe that after conjugation of the Tz-beads to EV-TCO, positivity in the PE channel remains constant. Also, the percentage of small particles (low f/s scatter) and big particles (high f/s scatter) being positive in the Pe channel does not change after the conjugation. Second, the percentage of high f/s scatter beads/complexes goes down significantly (p<0,05) after conjugation of the full system compared to the empty beads. Initially this seems to be counterintuitive, as complexes would become larger when conjugated to chemical groups or EVs. However, there is an explanation for this phenomenon with its origins in the acquisition of the FACS data. Each time FACS was performed, the naked bead samples were abundantly present while the conjugated beads were only 5µL in volume. To speed up the FACS data acquisition the empty beads were less diluted leading to a faster acquisition of events, but also elevating the concentration of particles in the sample tube. This increased concentration might be the explanation for a higher degree of clustering of beads, leading to a higher percentage of high f/s scattering events. To confirm this hypothesis a test should be set up in which the volumes of conjugated and non-conjugated beads are kept equal. Third, the Calcein staining, similar to the Tz-conjugation, is significantly higher for high f/s scattering particles compared to low f/s scattering particles.

*Table 5: Percentages of positive events for different gating strategies. Comparing empty beads with Tz conjugated beads and the two systems with antibodies (ASGR1 and EpCAM).*

| | Empty beads (n=4) | Beads-TZ (n=4) | System EpCAM (n=3) | System ASGR1 (n=3) |
|---|---|---|---|---|
| **TZ-Conjugation (overall)** | 0,23%±0,13 | 25,45%±4,29 | 22,93%±3,12 | 23,43%±4,99 |
| **Calcein-AM conjugation (overall)** | 0,08%±0,1 | 0,05%±0,1 | 9,93%±8,89 | 15,60%±10,76 |
| **Double positive** | 0,83%±0,5 | 0,18%±0,29 | 11,43%±2,94 | 12,83%±4,46 |
| **High f/s scatter** | 22,58%±3,29 | 18,83%±2,99 | 15,53%±2,42 | 16,20%±2,34 |
| **Low f/s scatter** | 77,42%±3,29 | 81,17%±2,99 | 84,47%±2,42 | 83,80%±2,34 |
| **High f/s scatter + TZ positive** | 0,73%±0,48 | 56,88%±3,73 | 61,80%±3,69 | 60,23%±7,75 |
| **Low f/s scatter + TZ positive** | 0,03%±0,05 | 18,15%±2,74 | 15,73%±1,78 | 16,23%±3,24 |
| **High f/s scatter + Calcein positive** | 0,28%±0,24 | 0,08%±0,05 | 31,83%±24,57 | 44,20%±27,05 |
| **Low f/s scatter + Calcein positive** | 0,00%±0,00 | 0,05%±0,1 | 5,6%±5,28 | 9,70%±6,95 |
| **High f/s scatter + Double positive** | 3,20%±1,73 | 0,73%±0,99 | 54,23%±4,04 | 53,40%±8,17 |
| **Low f/s scatter + Double positive** | 0,05%±0,06 | 0,05%±0,1 | 3,57%±1,51 | 4,87%±2,48 |

Additionally to the results displayed in the table, the FACS plots, displayed in Figure 22, provide alternative insights to the conjugation of the system. All ASGR1 plots are visualised with the FITC channel (ex 488 ; em 530/30) plotted against the side scatter of the events. Interestingly, you see that two measurements have nearly identical shapes (Figure 22c & 22d) (and also percentages of positive FITC events) and that one measurement is different (Figure 22e). Using the current gating strategy this one measurement would be classified as “failed or bad” conjugation. However, when we compare the failed (n=3) measurement with the empty magnetic beads, we see that the bulk of the events still display a clear shift to the right in the FITC channel. Therefore, this conjugation would not be classified as “failed”, only as being less pronounced then the other two measurements. The underlying cause of this difference is hard to determine. When thinking of possible variable parameters, the initial hypothesis would be that EV count in the sample from the HepG2 cells would is different, as it is the only changed variable compared to the other groups. Although this hypothesis can neither be denied or confirmed, due to the absence of the NTA measurement system, this hypothesis seems unlikely to be true as there was no clear difference in initial cell counts of the HepG2 cells after EV harvesting (1,3-1,4*10^6 cells/ml). An alternative explanation could be that in some cases the beads would agglomerate during the mixing on the roller mixer, and stick to the side of the Eppendorf tube, hindering mixing and possibly altering the conjugation efficiency. This phenomenon was observed several times when performing the conjugation, however this is not always detectable at the end of the mixing procedure as the beads would sink again when in upright position. Contradictory, the “failed” (n=3) beads had a lower percentage of high f/s scattering events, making this hypothesis unlikely to be the cause of the decreased conjugation. In this section the example of the ASPGR1 measurements is used, however the same holds for the EpCAM measurements with the only remark that in those measurements there were two so called “less pronounced” conjugations and one with higher conjugation efficiency.

The second gating strategy, which indicates particles that are both Pe and FITC positive according to the gates set in Chapter 4.12, provided some alternative insights on the FACS results. From Table 5, it

can be observed that this gating strategy mitigates the enormous differences between “failed” and “successful” conjugation. Additionally, the standard deviation of the second gating strategy is lower, allowing more differentiability between measurement groups. The reasoning behind the double positive gate is that the EVs can only, in principle, be captured by beads that are containing the Tz group resulting in a positive signal in both PE and FITC.

When evaluating the effect of the high f/s scatter with respect to the second gating strategy of “double positive” , the same effect is observed as with the separate gates for Tz and Calcein. The high f/s scatter events have a significantly higher percentage 54,23%±4,04 (EpCAM) and 53,40%±8,17 (ASGR1) of double positive signals compared to the low f/s scatter events 3,57%±1,51 (EpCAM) and 4,87%±2,48 (ASGR1). It should be noted that the “double positive” signal in the high f/s scattering beads probably is overestimated with this gating strategy as can be seen from the relatively high percentage for the empty beads (3,20%±1,73). The reason for such an overestimation could be because Pe and FITC channels slightly overlap allowing one signal (Calcein EV) to be positive in both channels. These overlapping FITC/Pe signals could therefore lead to an overestimation of the percentage of double positive beads. The overlapping FITC/Pe signals can be seen as the straight diagonal line in the PE versus FITC plots, as can be seen in Figure 24. These signals being accidentally marked “double positive” while in fact they are only Calcein positive is also clearly seen from the Calcein stained EV controls, also displayed in Figure 24.

On the contrary, a different (negative) effect of this gating strategy could lead to an underestimation of the double positive percentage, as EVs might overshadow the illuminated PE signal of the Tz group to which they are attached to. In this case the particles are indicated as “not double positive” when in fact, they should be. The physical blocking of the Pe signal, from reaching the FACS detector, by EVs can be called a shadowing effect.

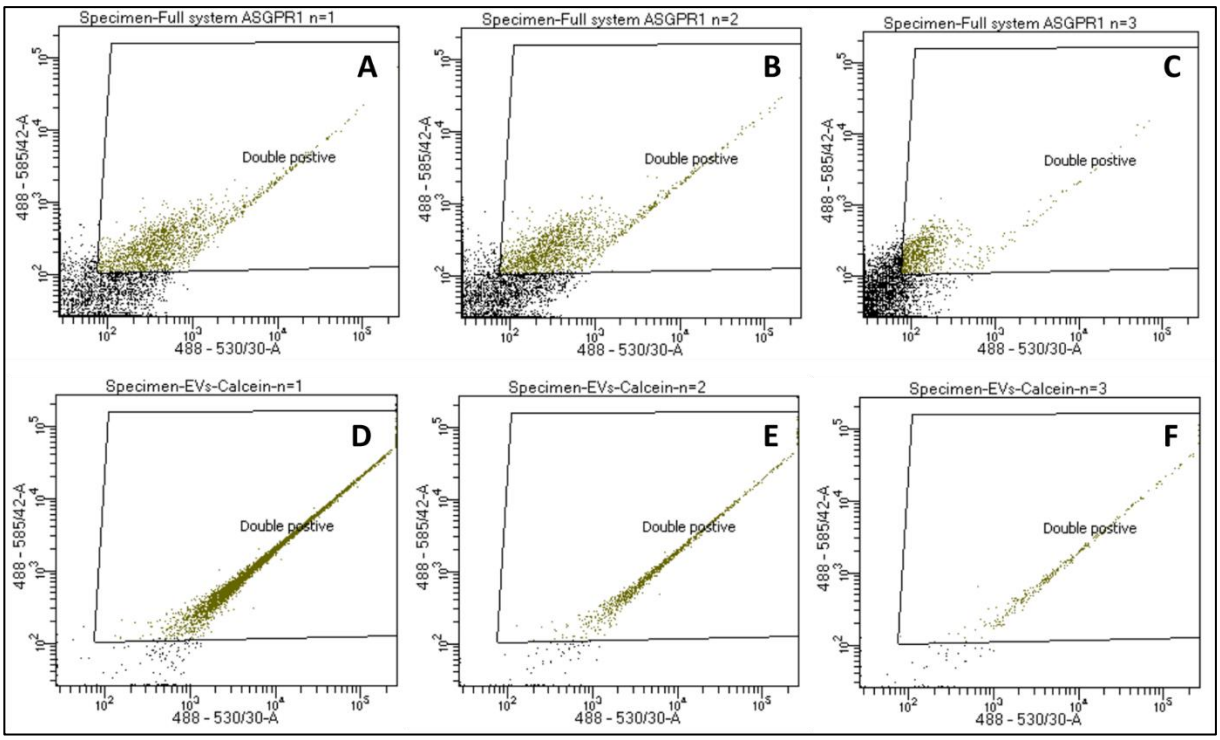


*Figure 24: Results obtained using “double positive” gating strategy. (A, B&C) Systems with ASGR1 antibody that captured Calcein stained EVs showed populations of double positives that were not on the diagonal line, (which suggests overlap in Pe and FITC channel) suggesting effective capture of Calcein stained EVs with beads that also contain Tz. (D, E&F) Calcein stained EVs confirm that Pe and FITC channel overlap and that EVs can be seen in both channels as a diagonal line.*

Interestingly, as can be seen from the top three pictures in supplementary Figure 4 corresponding to the fully conjugated systems with ASGR1 antibody, the high f/s scattering particles have a clear population of “double positive” events that do not lie near the diagonal line. On the contrary, the “double positive” events belonging to the low f/s scattering beads are mainly located on, or slightly next to, the diagonal line that indicates channel overlap. These results would suggest that the high f/s scattering population in the “double positive” gate, would be closer to being really positive in both Pe and FITC without overlapping of the channels. However, is should be mentioned that granularity and size could potentially also alter the magnitude of the shadowing effect between the Tz groups and EVs.

Results are solely based on FACS, as the magnetic beads are visible in the FITC channel on the FACS but not in the FITC channel under the microscope. To provide an uniform translation of the results the gating strategy is kept equal to the gating strategy for the previously conjugated parts (see 4.3). In general, flow cytometry is more sensitive than microscopic imaging resulting in the different detection by the two techniques [74]. Consequently, a possible reason for the beads-EVs being positive under the FACS but invisible in the FITC channel under the microscope might be because of the significant size difference between the magnetic beads and the EVs. The difference in size could lead to signal quenching or a shadowing effect of the beads towards the positive FITC signal of the EVs, weakening the FITC signal. As a consequence, the FITC signal is only detectable through flow cytometry, while it remains invisible in microscopy.

## 5.3 Improving the system

The outcomes presented in the preceding chapter confirm the feasibility and potential this magnetic bead-antibody system as a robust platform for targeted detection of biomolecules. Specifically, the results provide compelling evidence of the system's effectiveness in capturing and detecting HepG2 derived EVs through the utilization of magnetic beads conjugated with antibodies ASPGR1 and EpCAM. However, despite these promising outcomes, there are still areas for improvement that need to be addressed to fully exploit the capabilities of the magnetic bead-antibody system. In this section, the results of our systematic efforts to enhance the performance of the system will be presented. Furthermore, the feature of releasing the EVs will be presented and explained.

### 5.3.1 Optimization of concentration/volumes

After some initial attempts of conjugating the system, it was concluded that the antibody concentration of 0,5µg/ml was too low to facilitate successful conjugation to TCO. Beforehand, the TCO-antibody conjugation reaction was envisioned to be the slowest reaction of the whole conjugation [75]. When antibody concentration was increased to 10µg/ml, the system conjugation was consistently positive, although sometimes more pronounced than others (as explained in 4.2). Further optimization of antibody concentration might improve the system conjugation more, however this is a time and resource consuming practise and therefore left out of the scope of this research.

Volumes/concentration of OPSS-PEG5-NHS and 6-Methyl-Tetrazine-PEG5-NHS in the reaction mixtures were varied in experiments to check if it would impact the conjugation of the system. However, this was not the case, therefore it was decided to keep all concentrations equal to manufacturer’s instructions.

### 5.3.2 Sorting

In chapter 4.2.1, it becomes evident that successful conjugation of magnetic beads to Tz can be achieved, but this conjugation is far from ideal, as the conjugation is between 20-30 %. Optimally, one would want a 100 % conjugation. To purify the conjugated beads from the non-conjugated

beads, the gates were used for FACS sorting, based on positivity in the Pe channel. After sorting it can be seen that Tz conjugation increases slightly to 32,1±2,9% from the earlier mentioned 25,45%±4,29. Although this increase is significant ($p<0,0,5$), the difference between pre-sorting and after sorting are not in line with expectations. Reasons on why the conjugation is not the expected 100% can vary. One explanation could be that beads are falsely classified as being Pe positive because they are adherend to positive beads, and therefore are counted as a single positive event. A different explanation could be that the electrical forces used for FACS sorting might alter the chemical structure, causing previously Tz conjugated beads to lose their functionalisation group. Further research is needed to confirm or deny these statements and optimize the sorting procedure accordingly.

### 5.3.3 Release of the EVs

When the system is successful and captures the small EVs out of the conditioned medium, an important additional feature of the system enables downstream analysis of the EVs. This feature originates from the cleavable disulphide bridge between the original magnetic beads and their linker groups. In theory, one would add dithiothreitol (DTT) reducing the disulphide bridges thereby uncoupling the small EVs from their relatively large magnetic beads. The free EVs could then be analysed using techniques such as Western Blot and/or qPCR to get a better understanding of HCC pathophysiology. Furthermore, using NTA or fluorescence plate readers, efficiency of the capturing system could be determined. This would enable to vary parameters and see the effect on capturing efficiency directly, making it easier to tune and optimize the system.

The principle of release has been tested and results are displayed in Figure 25. In these results (N=2), release of the Tz group after initial conjugation is confirmed after 60 minutes of DTT treatment. In both cases, the positivity in Pe channel went from below 1% to about 10-20% (fast measured) and after DTT treatment back down to below 1%. It should be noted however that high concentrations of DTT could reduce disulphide bridges in other places of the biological sample as well, influencing for instance membrane stability. Membrane stability is very important to maintain in this particular system as when membranes are ruptured, Calcein can escape the EVs rendering them undetectable. Furthermore the leaked Calcein could stick to the magnetic beads, leading to false positive signals in the FITC channel. Additionally altered membrane structures could decrease translatability of the downstream analysis after capturing as the EVs would lose their integrity and structure.

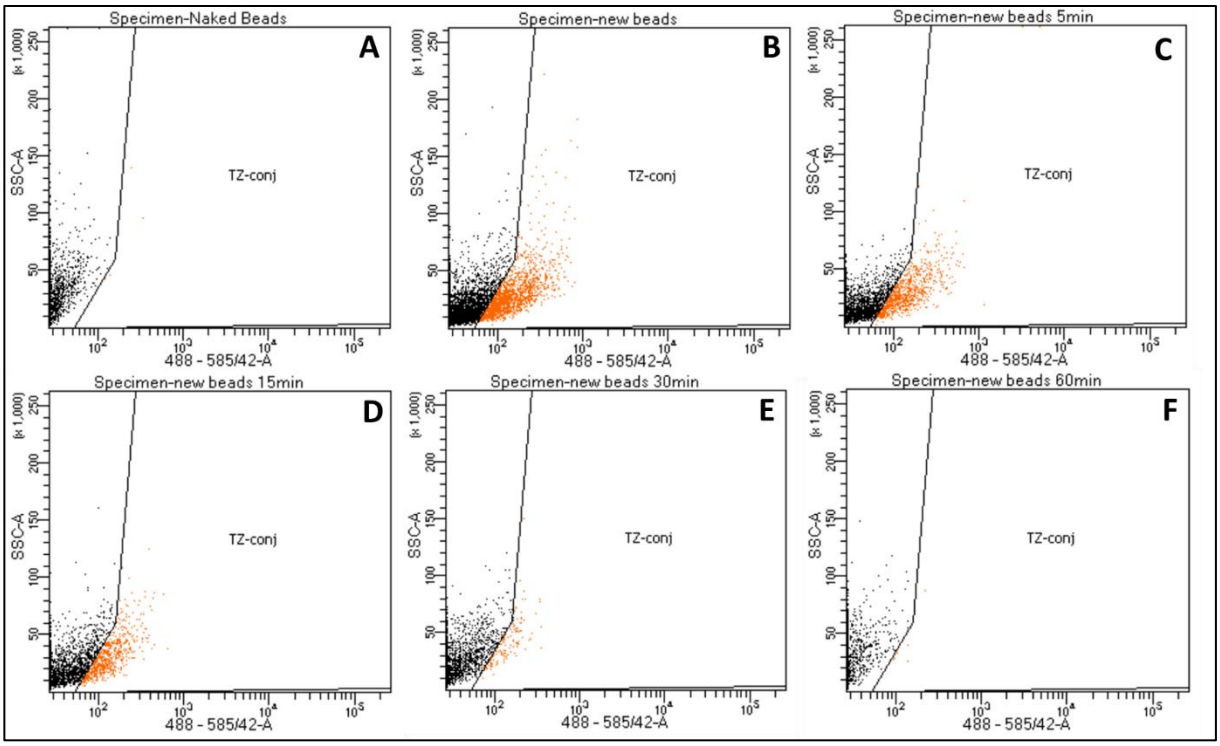


*Figure 25: Results of the DTT mediated release of the Tz groups from Tz conjugated beads by reducing the disulphide bonds. (A) Empty beads before conjugation to Tz. (B) Tz conjugated beads before DTT treatment. (C) Tz conjugated beads after 5 minutes of DTT treatment. (D) Tz conjugated beads after 15 minutes of DTT treatment. (E) Tz conjugated beads after 30 minutes of DTT treatment. (F) Tz conjugated beads after 60 minutes of DTT treatment. The plots show an increase of Pe positivity when conjugation Tz, following a gradual time-dependent decrease after DTT treatment is started.*

# 6. General discussion

The results and discussion section contained a lot of details, therefore this chapter tries to highlight the main results to identify interrelations and connections between different experiments and earlier published literature. The subdivision made is therefore only related to the main objectives of the research.

## 6.1 Characterisation of EVs

In this subchapter, the results of the different kinds of EV characterisation techniques will be discussed. The results will be compared, to each other and to results found in other papers, to determine if the initial sample of conditioned medium contained HCC derived EVs.

The results obtained by NTA confirmed particles predominantly in the size range between 50 nm and 300 nm, which is a typical size range for EVs. In a different paper, in which HepG2 derived EVs were isolated, the NTA particle size distribution plots supported the find that particles existed predominantly in the size range between 50 nm and 300 nm [76]. Additionally, Cryo-TEM pictures in both results sections (this research and research of Koenen et, al.) confirm lipid bilayer structures in this typical size range with morphology mimicking EV morphology. NTA results also showed particle counts of $(1{,}73\pm0{,}66)*10^{8}$ particles per ml of conditioned medium sample, which is relatively low compared to other research [33]. The lower particle counts can be caused by differences in collection/isolation protocols for obtaining EVs out of conditioned medium. Most EV research in which NTA is performed, ultracentrifugation is used to form a pellet of EVs and this pellet is resuspended in a very small volume of buffer solution. An advantage of this technique is that particle (EV) concentration is relatively high as when using ultracentrifugation it is way easier to remove the fluid supernatant and concentrate the sample compared to TFF. However a negative of this method, and thereby also the reason why it was not used in this research, is that by ultracentrifugation the integrity and stability of EVs might change hampering translatability in the further characterisation process. Due to these reasons particle counts presented in this research are difficult to compare with other papers.

Information on the protein contents of the EVs was gathered by both Western blot and Dot blot. Western blot and Dot blot both confirmed presence of ASGR1 and CD9, which was similar to what was found in literature [41]. The EpCAM was different for both, where expression in Dot Blot was very high, the expression in Western blot was zero. Reasons for this could be the difference between nitrocellulose and PVDF membranes, as the Dot blot expressions where a higher in general. A different reason could be that the Western blot only consisted of a primary and a secondary antibody compared to the Dot blot (which had tertiary antibodies as well). Finally, the missing EpCAM expression could just be a pipetting error in the Western Blot as the volume of antibody in the solution was relatively small (0,14µL in 1mL). In literature, EpCAM expression in HepG2 derived EVs is widely reported supporting the suggestion of an error in the Western blot [7,41,65].

When evaluating the Calcein staining, the results of both microscopy and FACS are in line with each other and expectations based on literature [52]. Indicating successful Calcein staining of the EVs in all samples.

## 6.2 Conjugation of the subparts of the system

In this subchapter the results regarding successful conjugation of the subparts of the capturing system are discussed.

Both microscopy and FACS results indicate successful conjugation of the subparts of the system. The Tz autofluorescence is seen in the Pe channel of the FACS and microscopy after conjugation reaction were performed. The results are also in accordance with the earlier found literature [60]. Although successful the conjugation efficiency of 25,45%±4,29 is low when compared to commercially available functionalised magnetic beads. Furthermore, it was indicated that larger beads (high f/s scatter) had higher Tz conjugation. This can be explained by their higher surface area, providing more possible thiol binding sites for the initial reaction, and subsequently providing more amine ($NH_2$) binding sites in the following reaction.

## 6.3 Capturing of the HCC derived EVs

In this subchapter the results regarding the capturing of HCC derived EVs by the system will be discussed.

The FACS results showed that the system was able to capture HCC derived EVs. The percentage of beads conjugated to Calcein stained EVs was 9,93%±8,89 and 15,60%±10,76 for EpCAM and ASGR1 antibodies respectively. Furthermore, results showed that larger particles (high f/s scatter) had higher conjugation to EVs. A reason for it could be that, because antibodies can have more than one TCO group attached to them, more than one magnetic bead is coupled to a single EV. A different reason could be because the larger beads also had a higher conjugation to Tz, offering a higher chance of capturing EVs.

## 6.4 Improving of the system

In this chapter the results regarding the improvement of the system based on gained knowledge into its capturing efficiency will be discussed.

The optimization of the system gained insights on the structure and reaction dynamics of the system. In initial experiments the conjugation of TCO to antibodies was deemed to be the cause of failure of the capturing system. When relating the optimization problem to the already performed conjugation reactions, it could be seen that the reaction between Ab and TCO is the same reaction as the reaction between -$NH_2$ and NHS of the OPSS group and the Tz group when conjugating the magnetic beads. The main difference in protocol was the pH, which was suboptimal for the Ab-TCO conjugation. Subsequently, by creating an overload of antibody to TCO the problem was solved.

The results of optimization by sorting the Tz beads did show a significant increase in Tz conjugation however it should be questioned if the sorting of the beads with these settings is worth the time and effort, as FACS sorting takes time to calibrate and perform while the results are only slightly better. Further research is needed to optimize the sorting procedure.

The results of the additional feature of release were promising but need further research to confirm made statements. Furthermore it should be evaluated if subjecting the EVs to DTT alters their integrity as proposed by earlier published literature [77].

# 7. Conclusion

The aim of this research was is to develop a capturing system that is capable of specifically capturing HCC derived EVs from conditioned cell medium. To do so, we developed a system based on magnetic beads covalently conjugated to antibodies.

In order to draw conclusions about the success of this capturing system, we first needed to be sure that HCC derived EVs were actually present in the conditioned cell medium. When combing our findings from different EV characterisation techniques, and comparing them with previously published literature, initial presence of HCC derived EVs in conditioned cell medium can be confirmed. The findings indicated the presence of lipid bilayer structures with sizes ranging between 50-300nm, expressing HCC derived EV markers EpCAM, ASGR1 and CD9.

Secondly, using fluorescent staining of the EVs, our FACS based findings indicated a significant increase in FITC and Pe positive signals after conjugation of the system. Indicating successful conjugation of the subparts, as well as confirming the capture of HCC derived EVs from conditioned cell medium. Some work was performed in trying to optimize the system and exploring additional features. Although the proof of concept of this work seems promising, more research is needed to confirm statements made on the capturing system. Moreover, quantifying efficiency of the capturing system remains challenging and needs additional research efforts.

# 8. Future recommendations

In this research a proof of concept is displayed of a capturing system that is able to selectively capture HCC derived EVs from cell culture medium. However, to broaden the scope of this concept and determine additional insights in efficiency future research is needed.

In characterisation of EVs needs optimization in a few different aspects. First, cryo-TEM should be repeated. While repeating the experiment, the concentration of EVs would need to be increased to get a more comprehensive picture of EV morphology and average size. To achieve this a lot of medium would need to be concentrated, so it has to be noted that this would be a time and resource consuming experiment. Secondly, NTA should be repeated with uncontaminated starvation medium. By using a new TFF column, and concentrating the starvation sample before the EV samples this could lead to a significant increase of particle detection when comparing EV samples with controls. Thirdly, the influence of RIPA buffer on Western blot results could be examined to test whether Calnexin is really absent in EV samples (meaning there are no cells). Furthermore, repeating Western blot would allow statistical analysis of the quantified proteins by comparing medium controls with cells and EV samples. Fourthly, the protocol of EV staining could be adjusted to add the Calcein-AM directly to the EV sample without first making the staining solution. In this case the sample of EVs would not be diluted by the PBS in the staining solution, which could ultimately lead to higher concentrations of EVs in the conjugation reaction with the TCO-antibodies and the Tz-beads. Lastly, to obtain a more complete picture of EV cargoes, polymerase chain reaction (PCR) analysis would be needed [65]. PCR enables the profiling of specific RNA species within EVs, facilitating the investigation of EV cargo and potential functional implications. The analysis would provide information on miRNAs, mRNAs, and non-coding RNAs, which can play crucial roles in cell-to-cell communication and disease processes [65].

In the conjugation of the subparts it is suggested that the effect of Antibody TCO conjugation at higher pH (8,5) should be tested, to see if this improves the system. Furthermore, it can be useful to outsource the production of Tz-beads to a specialised chemical manufacturing company. The hypothesis is that a more pure sample of Tz-beads would lead to higher conjugation efficiency of the total system by enabling more possible binding sites for the antibody-TCO. Alternatively, research could be aimed at improving the conjugation by itself. A possibility could be by using Ellman's' reagent to stain unreacted thiol groups of the magnetic beads, thereby indicating if Tz conjugation worked and how many room there is for improvement. Sorting of the beads could then be used to optimize the purity of Tz-beads. Different gating strategies for sorting should be tested as the current research has shown that sorting based on current gates is far from optimal.

Further research in the capturing of the EVs by the capturing system would be needed in more accurately determining the efficiency of the system. The unique feature of releasing the EVs could be useful for obtaining information on efficiency. However, although the principle of release was tested in Tz-beads, the feature needs to be tested on fully conjugated systems first. If release of the EVs is possible, downstream analysis of captured EVs would be helpful to determine the effects on integrity and to evaluate HCC derived EV purity compared to contaminants. Moreover, using the release feature of the EVs, experiments could be designed around NTA or fluorescence intensity readouts to make quantitative statements on how many (number or percentage wise) of the initial EVs are captured by the system.

When all of these parameters have been optimized, the system can be used for further research into its possible applications. For instance, the capturing system could be used to capture EVs from human blood plasma. In addition, because the concept of capturing has been proven, the capturing

system could be optimized for different cell type derived EVs using different antibodies for capturing. The ultimate goal would be that the system is applicable to every cell type and every antibody to capture EVs from human blood plasma.

# 9. Acknowledgements

In the first place I want to thank Dr. Ruchi Bansal and Richell Booijink for their supervision, expertise, flexibility and enthusiastic approach to support me with completing my master thesis. Next to that I want to thank them, and everyone else who worked at MCBP/BioEE somewhere between 2022-2023 for a wonderful time. Everyone was always ready to answer questions or help with experiments. In particular I want to thank Richell Booijink for her help with starvation of the EVs, and helping me get used to all different characterisation techniques in the lab. For the cryo-TEM experiments I want to thank Dr. Amit Khurana and Amber van Kampen for their willingness to take my samples with them to Groningen. Lastly, I want to thank Prof.dr.ir. Pascal Jonkheijm for being available for questions (especially chemistry related) and being a member of my exam committee.

# References


[1] Chidambaranathan-Reghupaty S, Fisher PB, Sarkar D. Hepatocellular carcinoma (HCC): Epidemiology, etiology and molecular classification. Advances in Cancer Research 2021;149:1. doi:10.1016/BS.ACR.2020.10.001.

[2] Singh AK, Kumar R, Pandey AK. Hepatocellular Carcinoma: Causes, Mechanism of Progression and Biomarkers. Current Chemical Genomics and Translational Medicine 2018;12:9. doi:10.2174/2213988501812010009.

[3] Kumari R, Sahu MK, Tripathy A, Uthansingh K, Behera M. Hepatocellular carcinoma treatment: hurdles, advances and prospects. Hepatic Oncology 2018;5:HEP08. doi:10.2217/HEP-2018-0002.

[4] Ahn JC, Lee Y Te, Agopian VG, Zhu Y, You S, Tseng HR, Yang JD. Hepatocellular carcinoma surveillance: current practice and future directions. Hepatoma Research 2022;8:10. doi:10.20517/2394-5079.2021.131.

[5] Yang JD, Heimbach JK. New advances in the diagnosis and management of hepatocellular carcinoma. BMJ (Clinical Research Ed) 2020;371. doi:10.1136/BMJ.M3544.

[6] Ayoub WS, Steggerda J, Yang JD, Kuo A, Sundaram V, Lu SC. Current status of hepatocellular carcinoma detection: screeningstrategies and novel biomarkers. Therapeutic Advances in Medical Oncology 2019;11. doi:10.1177/1758835919869120.

[7] Galle PR, Foerster F, Kudo M, Chan SL, Llovet JM, Qin S, Schelman WR, Chintharlapalli S, Abada PB, Sherman M, Zhu AX. Biology and significance of alpha-fetoprotein in hepatocellular carcinoma. Liver International 2019;39:2214–29. doi:10.1111/LIV.14223.

[8] Zhang J, Chen G, Zhang P, Zhang J, Li X, Gan D, Cao X, Han M, Du H, Ye Y. The threshold of alpha-fetoprotein (AFP) for the diagnosis of hepatocellular carcinoma: A systematic review and meta-analysis. PLOS ONE 2020;15:e0228857. doi:10.1371/JOURNAL.PONE.0228857.

[9] Nowicki TK, Markiet K, Szurowska E. Diagnostic Imaging of Hepatocellular Carcinoma - A Pictorial Essay. Current Medical Imaging Reviews 2017;13:140. doi:10.2174/1573405612666160720123748.

[10] Lone SN, Nisar S, Masoodi T, Singh M, Rizwan A, Hashem S, El-Rifai W, Bedognetti D, Batra SK, Haris M, Bhat AA, Macha MA. Liquid biopsy: a step closer to transform diagnosis, prognosis and future of cancer treatments. Molecular Cancer 2022 21:1 2022;21:1–22. doi:10.1186/S12943-022-01543-7.

[11] Pan Y, Chen H, Yu J. Biomarkers in Hepatocellular Carcinoma: Current Status and Future Perspectives. Biomedicines 2020;8:1–17. doi:10.3390/BIOMEDICINES8120576.

[12] Lou J, Zhang L, Lv S, Zhang C, Jiang S. Biomarkers for Hepatocellular Carcinoma. Https://DoiOrg/101177/1179299X16684640 2017;53:403–22. doi:10.1177/1179299X16684640.

[13] Gowhari A, Phd S, Fatemeh Ezzatifar |, Aravindhan S, Angelina |, Zekiy O, Majid |, Phd A, Seyed |, Gheibihayat M, Jamshid |, Navashenaq G, Navashenaq JG. Shedding more light on the role of Midkine in hepatocellular carcinoma: New perspectives on diagnosis and therapy. IUBMB Life 2021;73:659–69. doi:10.1002/IUB.2458.

[14] Zhu M, Zheng J, Wu F, Kang B, Liang J, Heskia F, Zhang X, Shan Y. OPN is a promising serological biomarker for hepatocellular carcinoma diagnosis. Journal of Medical Virology 2020;92:3596–603. doi:10.1002/JMV.25704.

[15] Liu CH, Gil-Gómez A, Ampuero J, Romero-Gómez M. Diagnostic accuracy of SCCA and SCCA-IgM for hepatocellular carcinoma: A meta-analysis. Liver International 2018;38:1820–31. doi:10.1111/LIV.13867.

[16] Chuo STY, Chien JCY, Lai CPK. Imaging extracellular vesicles: Current and emerging methods. Journal of Biomedical Science 2018;25:1–10. doi:10.1186/S12929-018-0494-5/FIGURES/3.

[17] Anand S, Samuel M, Mathivanan S. Exomeres: A New Member of Extracellular Vesicles Family. Subcellular Biochemistry 2021;97:89–97. doi:10.1007/978-3-030-67171-6_5/FIGURES/1.

[18] Zhao Z, Wijerathne H, Godwin AK, Soper SA. Isolation and analysis methods of extracellular vesicles (EVs). Extracellular Vesicles and Circulating Nucleic Acids 2021;2:80–103. doi:10.20517/EVCNA.2021.07.

[19] Doyle LM, Wang MZ. Overview of Extracellular Vesicles, Their Origin, Composition, Purpose, and Methods for Exosome Isolation and Analysis. Cells 2019;8. doi:10.3390/CELLS8070727.

[20] Chen Y, Yu L. Extracellular vesicles: from bench to bedside. Current Medicine 2022 1:1 2022;1:1–12. doi:10.1007/S44194-022-00001-2.

[21] Hu T, Wolfram J, Srivastava S. Extracellular Vesicles in Cancer Detection: Hopes and Hypes. Trends in Cancer 2021;7:122–33. doi:10.1016/J.TRECAN.2020.09.003.

[22] Willms E, Cabañas C, Mäger I, Wood MJA, Vader P. Extracellular vesicle heterogeneity: Subpopulations, isolation techniques, and diverse functions in cancer progression. Frontiers in Immunology 2018;9:738. doi:10.3389/FIMMU.2018.00738/BIBTEX.

[23] Szatanek R, Baj-Krzyworzeka M, Zimoch J, Lekka M, Siedlar M, Baran J. The Methods of Choice for Extracellular Vesicles (EVs) Characterization. International Journal of Molecular Sciences 2017;18. doi:10.3390/IJMS18061153.

[24] Yokoi A, Ochiya T. Exosomes and extracellular vesicles: Rethinking the essential values in cancer biology. Seminars in Cancer Biology 2021;74:79–91. doi:10.1016/J.SEMCANCER.2021.03.032.

[25] Nanou A, Miller MC, Zeune LL, de Wit S, Punt CJA, Groen HJM, Hayes DF, de Bono JS, Terstappen LWMM. Tumour-derived extracellular vesicles in blood of metastatic cancer patients associate with overall survival. British Journal of Cancer 2020 122:6 2020;122:801–11. doi:10.1038/s41416-019-0726-9.

[26] Anand S, Samuel M, Kumar S, Mathivanan S. Ticket to a bubble ride: Cargo sorting into exosomes and extracellular vesicles. Biochimica et Biophysica Acta (BBA) - Proteins and Proteomics 2019;1867:140203. doi:10.1016/J.BBAPAP.2019.02.005.

[27] Liangsupree T, Multia E, Riekkola ML. Modern isolation and separation techniques for extracellular vesicles. Journal of Chromatography A 2021;1636:461773. doi:10.1016/J.CHROMA.2020.461773.

[28] Busatto S, Vilanilam G, Ticer T, Lin WL, Dickson DW, Shapiro S, Bergese P, Wolfram J. Tangential Flow Filtration for Highly Efficient Concentration of Extracellular Vesicles from Large Volumes of Fluid. Cells 2018;7:273. doi:10.3390/CELLS7120273.

[29] Brennan K, Martin K, FitzGerald SP, O'Sullivan J, Wu Y, Blanco A, Richardson C, Mc Gee MM. A comparison of methods for the isolation and separation of extracellular vesicles from protein and lipid particles in human serum. Scientific Reports 2020 10:1 2020;10:1–13. doi:10.1038/s41598-020-57497-7.

[30] Karttunen J, Heiskanen M, Navarro-Ferrandis V, Das Gupta S, Lipponen A, Puhakka N, Rilla K,

Koistinen A, Pitkänen A. Precipitation-based extracellular vesicle isolation from rat plasma co-precipitate vesicle-free microRNAs. Journal of Extracellular Vesicles 2019;8. doi:10.1080/20013078.2018.1555410/SUPPL_FILE/ZJEV_A_1555410_SM5690.DOCX.

[31] Logozzi M, Di Raimo R, Mizzoni D, Fais S. Immunocapture-based ELISA to characterize and quantify exosomes in both cell culture supernatants and body fluids. Methods in Enzymology 2020;645:155. doi:10.1016/BS.MIE.2020.06.011.

[32] Mathew DG, Beekman P, Lemay SG, Zuilhof H, Le Gac S, Van Der Wiel WG. Electrochemical Detection of Tumor-Derived Extracellular Vesicles on Nanointerdigitated Electrodes. Nano Letters 2020;20:820–8. doi:10.1021/ACS.NANOLETT.9B02741/SUPPL_FILE/NL9B02741_SI_002.PDF.

[33] Gámez-Valero A, Monguió-Tortajada M, Carreras-Planella L, Franquesa M, Beyer K, Borràs FE. Size-Exclusion Chromatography-based isolation minimally alters Extracellular Vesicles' characteristics compared to precipitating agents. Scientific Reports 2016 6:1 2016;6:1–9. doi:10.1038/srep33641.

[34] Schulze RJ, Schott MB, Casey CA, Tuma PL, McNiven MA. Beyond the Cell: The cell biology of the hepatocyte: A membrane trafficking machine. The Journal of Cell Biology 2019;218:2096. doi:10.1083/JCB.201903090.

[35] Lee Y Te, Tran B V., Wang JJ, Liang IY, You S, Zhu Y, Agopian VG, Tseng HR, Yang JD. The Role of Extracellular Vesicles in Disease Progression and Detection of Hepatocellular Carcinoma. Cancers 2021, Vol 13, Page 3076 2021;13:3076. doi:10.3390/CANCERS13123076.

[36] Královec K, Melounková L, Slováková M, Mannová N, Sedlák M, Bartáček J, Havelek R. Disruption of Cell Adhesion and Cytoskeletal Networks by Thiol-Functionalized Silica-Coated Iron Oxide Nanoparticles. International Journal of Molecular Sciences 2020, Vol 21, Page 9350 2020;21:9350. doi:10.3390/IJMS21249350.

[37] Altinbasak I, Arslan M, Sanyal R, Sanyal A. Pyridyl disulfide-based thiol–disulfide exchange reaction: shaping the design of redox-responsive polymeric materials. Polymer Chemistry 2020;11:7603–24. doi:10.1039/D0PY01215G.

[38] Hermanson GT. (Strept)avidin–Biotin Systems. Bioconjugate Techniques 2013:465–505. doi:10.1016/B978-0-12-382239-0.00011-X.

[39] Eslami-S Z, Cortés-Hernández LE, Alix-Panabières C. Epithelial Cell Adhesion Molecule: An Anchor to Isolate Clinically Relevant Circulating Tumor Cells. Cells 2020, Vol 9, Page 1836 2020;9:1836. doi:10.3390/CELLS9081836.

[40] Nanou A, Zeune LL, Terstappen LWMM. Leukocyte-Derived Extracellular Vesicles in Blood with and without EpCAM Enrichment. Cells 2019;8. doi:10.3390/CELLS8080937.

[41] Julich-Haertel H, Urban SK, Krawczyk M, Willms A, Jankowski K, Patkowski W, Kruk B, Krasnodębski M, Ligocka J, Schwab R, Richardsen I, Schaaf S, Klein A, Gehlert S, Sänger H, Casper M, Banales JM, … Kornek M. Cancer-associated circulating large extracellular vesicles in cholangiocarcinoma and hepatocellular carcinoma. Journal of Hepatology 2017;67:282–92. doi:10.1016/J.JHEP.2017.02.024.

[42] Roa-Colomo A, López Garrido MÁ, Molina-Vallejo P, Rojas A, Sanchez MG, Aranda-García V, Salmeron J, Romero-Gomez M, Muntane J, Padillo J, Alamo JM, Lorente JA, Serrano MJ, Garrido-Navas MC. Hepatocellular carcinoma risk-stratification based on ASGR1 in circulating epithelial cells for cancer interception. Frontiers in Molecular Biosciences 2022;9:1308. doi:10.3389/FMOLB.2022.1074277/BIBTEX.

[43] Patil US, Qu H, Caruntu D, O'Connor CJ, Sharma A, Cai Y, Tarr MA. Labeling Primary Amine Groups in Peptides and Proteins with N-Hydroxysuccinimidyl Ester Modified Fe3O4@SiO2 Nanoparticles Containing Cleavable Disulfide-bond Linkers. Bioconjugate Chemistry 2013;24:1562–9. doi:10.1021/BC400165R.

[44] Haraszti RA, Miller R, Dubuke ML, Rockwell HE, Coles AH, Sapp E, Didiot MC, Echeverria D, Stoppato M, Sere YY, Leszyk J, Alterman JF, Godinho BMDC, Hassler MR, McDaniel J, Narain NR, Wollacott R, … Khvorova A. Serum Deprivation of Mesenchymal Stem Cells Improves Exosome Activity and Alters Lipid and Protein Composition. IScience 2019;16:230–41. doi:10.1016/J.ISCI.2019.05.029.

[45] Béquignat JB, Ty N, Rondon A, Taiariol L, Degoul F, Canitrot D, Quintana M, Navarro-Teulon I, Miot-Noirault E, Boucheix C, Chezal JM, Moreau E. Optimization of IEDDA bioorthogonal system: Efficient process to improve trans-cyclooctene/tetrazine interaction. European Journal of Medicinal Chemistry 2020;203:112574. doi:10.1016/J.EJMECH.2020.112574.

[46] Smith ZJ, Lee C, Rojalin T, Carney RP, Hazari S, Knudson A, Lam K, Saari H, Ibañez EL, Viitala T, Laaksonen T, Yliperttula M, Wachsmann-Hogiu S. Single exosome study reveals subpopulations distributed among cell lines with variability related to membrane content. Journal of Extracellular Vesicles 2015;4:28533. doi:10.3402/JEV.V4.28533.

[47] Yuana Y, Koning RI, Kuil ME, Rensen PCN, Koster AJ, Bertina RM, Osanto S. Cryo-electron microscopy of extracellular vesicles in fresh plasma. Journal of Extracellular Vesicles 2013;2:21494. doi:10.3402/JEV.V2I0.21494.

[48] Han HM, Bouchet-Marquis C, Huebinger J, Grabenbauer M. Golgi apparatus analyzed by cryo-electron microscopy. Histochemistry and Cell Biology 2013;140:369–81. doi:10.1007/S00418-013-1136-3/FIGURES/3.

[49] Vestad B, Llorente A, Neurauter A, Phuyal S, Kierulf B, Kierulf P, Skotland T, Sandvig K, Haug KBF, Øvstebø R. Size and concentration analyses of extracellular vesicles by nanoparticle tracking analysis: a variation study. Journal of Extracellular Vesicles 2017;6. doi:10.1080/20013078.2017.1344087.

[50] Panagopoulou MS, Wark AW, Birch DJS, Gregory CD. Phenotypic analysis of extracellular vesicles: a review on the applications of fluorescence. Https://DoiOrg/101080/2001307820191710020 2020;9:1710020. doi:10.1080/20013078.2019.1710020.

[51] Balaj L, Boulanger CM, Carter DRF, Compeer EB, Angelo GD', Andaloussi E, Goetz JG, Gross JC, Hyenne V, Krämer-Albers E-M, Lai C, Loyer X, Marki A, Momma S, Nolte 't Hoen E, Michiel D, Peinado H, … Wubbolts R. The power of imaging to understand extracellular vesicle biology in vivo n.d. doi:10.1038/s41592-021-01206-3.

[52] Gray WD, Mitchell AJ, Searles CD. An accurate, precise method for general labeling of extracellular vesicles. MethodsX 2015;2:360. doi:10.1016/J.MEX.2015.08.002.

[53] Andreu Z, Yáñez-Mó M. Tetraspanins in Extracellular Vesicle Formation and Function. Frontiers in Immunology 2014;5. doi:10.3389/FIMMU.2014.00442.

[54] Khushman M, Bhardwaj A, Patel GK, Laurini JA, Roveda K, Tan MC, Patton MC, Singh S, Taylor W, Singh AP. Exosomal Markers (CD63 and CD9) Expression Pattern Using Immunohistochemistry in Resected Malignant and Non-malignant Pancreatic Specimens. Pancreas 2017;46:782. doi:10.1097/MPA.0000000000000847.

[55] Li X, Chen R, Kemper S, Brigstock DR. Extracellular Vesicles From Hepatocytes Are Therapeutic

for Toxin-Mediated Fibrosis and Gene Expression in the Liver. Frontiers in Cell and Developmental Biology 2020;7. doi:10.3389/FCELL.2019.00368/FULL.

[56] Ekström K, Crescitelli R, Pétursson HI, Johansson J, Lässer C, Bagge RO. Characterization of surface markers on extracellular vesicles isolated from lymphatic exudate from patients with breast cancer. BMC Cancer 2022;22:1–17. doi:10.1186/S12885-021-08870-W/FIGURES/5.

[57] Wang J, Wuethrich A, Sina AAI, Lane RE, Lin LL, Wang Y, Cebon J, Behren A, Trau M. Tracking extracellular vesicle phenotypic changes enables treatment monitoring in melanoma. Science Advances 2020;6. doi:10.1126/SCIADV.AAX3223.

[58] Yumnam S, Saralamma VVG, Raha S, Lee HJ, Lee WS, Kim EH, Lee SJ, Heo JD, Kim GS. Proteomic profiling of human HepG2 cells treated with hesperidin using antibody array. Molecular Medicine Reports 2017;16:5386. doi:10.3892/MMR.2017.7232.

[59] Brusse M. Isolation of hepatocellular carcinoma specific extracellular vesicles. Saxion University of Applied Sciences, 2021.

[60] Johann K, Svatunek D, Seidl C, Rizzelli S, Bauer TA, Braun L, Koynov K, Mikula H, Barz M. Tetrazine- and trans-cyclooctene-functionalised polypept(o)ides for fast bioorthogonal tetrazine ligation. Polymer Chemistry 2020;11:4396–407. doi:10.1039/D0PY00375A.

[61] Di Bella MA. Overview and Update on Extracellular Vesicles: Considerations on Exosomes and Their Application in Modern Medicine. Biology 2022, Vol 11, Page 804 2022;11:804. doi:10.3390/BIOLOGY11060804.

[62] Melo GB, da Cruz NFS, do Monte Agra LL, Emerson GG, Lima LH, Linkuviene V, Maia M, Farah ME, Carpenter JF, Rodrigues EB, Probst C. Silicone oil-free syringes, siliconized syringes and needles: quantitative assessment of silicone oil release with drugs used for intravitreal injection. Acta Ophthalmologica 2021;99:e1366–74. doi:10.1111/AOS.14838.

[63] Thompson RF, Walker M, Siebert CA, Muench SP, Ranson NA. An introduction to sample preparation and imaging by cryo-electron microscopy for structural biology. Methods 2016;100:3–15. doi:10.1016/J.YMETH.2016.02.017.

[64] Mahmood T, Yang PC. Western Blot: Technique, Theory, and Trouble Shooting. North American Journal of Medical Sciences 2012;4:429. doi:10.4103/1947-2714.100998.

[65] Sun N, Lee Y Te, Zhang RY, Kao R, Teng PC, Yang Y, Yang P, Wang JJ, Smalley M, Chen PJ, Kim M, Chou SJ, Bao L, Wang J, Zhang X, Qi D, Palomique J, … Zhu Y. Purification of HCC-specific extracellular vesicles on nanosubstrates for early HCC detection by digital scoring. Nature Communications 2020 11:1 2020;11:1–12. doi:10.1038/s41467-020-18311-0.

[66] Qiu X, Campos Y, van de Vlekkert D, Gomero E, Tanwar AC, Kalathur R, Weesner JA, Bongiovanni A, Demmers J, d'Azzo A. Distinct functions of dimeric and monomeric scaffold protein Alix in regulating F-actin assembly and loading of exosomal cargo. Journal of Biological Chemistry 2022;298:102425. doi:10.1016/J.JBC.2022.102425.

[67] Matsui T, Osaki F, Hiragi S, Sakamaki Y, Fukuda M. ALIX and ceramide differentially control polarized small extracellular vesicle release from epithelial cells. EMBO Reports 2021;22:e51475. doi:10.15252/EMBR.202051475.

[68] Larios J, Mercier V, Roux A, Gruenberg J. ALIX- and ESCRT-III–dependent sorting of tetraspanins to exosomes. The Journal of Cell Biology 2020;219. doi:10.1083/JCB.201904113.

[69] Van Deun J, Mestdagh P, Sormunen R, Cocquyt V, Vermaelen K, Vandesompele J, Bracke M, De Wever O, Hendrix A. The impact of disparate isolation methods for extracellular vesicles on

downstream RNA profiling. Journal of Extracellular Vesicles 2014;3. doi:10.3402/JEV.V3.24858/SUPPL_FILE/ZJEV_A_11815517_SM0001.PDF.

[70] Adriaenssens E, Asselbergh B, Rivera-Mejías P, Bervoets S, Vendredy L, De Winter V, Spaas K, de Rycke R, van Isterdael G, Impens F, Langer T, Timmerman V. Small heat shock proteins operate as molecular chaperones in the mitochondrial intermembrane space. Nature Cell Biology 2023 25:3 2023;25:467–80. doi:10.1038/s41556-022-01074-9.

[71] Wang C, Zhang Y, Guo K, Wang N, Jin H, Liu Y, Qin W. Heat shock proteins in hepatocellular carcinoma: Molecular mechanism and therapeutic potential. International Journal of Cancer 2016;138:1824–34. doi:10.1002/IJC.29723.

[72] Hryciw DH, Wang Y, Devuyst O, Pollock CA, Poronnik P, Guggino WB. Cofilin Interacts with ClC-5 and Regulates Albumin Uptake in Proximal Tubule Cell Lines. Journal of Biological Chemistry 2003;278:40169–76. doi:10.1074/JBC.M307890200.

[73] Midekessa G, Godakumara K, Ord J, Viil J, Lättekivi F, Dissanayake K, Kopanchuk S, Rinken A, Andronowska A, Bhattacharjee S, Rinken T, Fazeli A. Zeta Potential of Extracellular Vesicles: Toward Understanding the Attributes that Determine Colloidal Stability. ACS Omega 2020;5:16701–10. doi:10.1021/ACSOMEGA.0C01582/SUPPL_FILE/AO0C01582_SI_003.AVI.

[74] Stachurska A, Gmerek K, Fabijańska-Mitek J. Experimental immunology - Application of flow cytometry and microscopy methods in erythrophagocytosis measurement. Central European Journal of Immunology 2013;38:208–13. doi:10.5114/CEJI.2013.35217.

[75] Lim CY, Owens NA, Wampler RD, Ying Y, Granger JH, Porter MD, Takahashi M, Shimazu K. Succinimidyl ester surface chemistry: Implications of the competition between aminolysis and hydrolysis on covalent protein immobilization. Langmuir 2014;30:12868–78. doi:10.1021/LA503439G/ASSET/IMAGES/LARGE/LA-2014-03439G_0009.JPEG.

[76] Koenen MT, Brandt EF, Kaczor DM, Caspers T, Heinzmann ACA, Fischer P, Heinrichs D, Wirtz TH, Trautwein C, Koenen RR, Berres ML. Extracellular Vesicles from Steatotic Hepatocytes Provoke Pro-Fibrotic Responses in Cultured Stellate Cells. Biomolecules 2022;12:698. doi:10.3390/BIOM12050698/S1.

[77] Konoshenko MY, Lekchnov EA, Vlassov A V., Laktionov PP. Isolation of Extracellular Vesicles: General Methodologies and Latest Trends. BioMed Research International 2018;2018. doi:10.1155/2018/8545347.

# Supplementary data

*Supplementary Table 1: Information on antibodies used in Dot blot and Western blot. Suppliers, species, dilutions and catalogue numbers.*

| Primary antibodies | Supplier | Species | Dilution | Cat. number |
|---|---|---|---|---|
| ASGR1 | Invitrogen | Rabbit | 1:1000 | PA5-52885 |
| EpCAM | Hansa Biomed | Rabbit | 1:7000 | PSK-A5 |
| CD9 | Hansa Biomed | Mouse | 1:10000 | HBM-CD9-100 |
| Calnexin | Cell signalling technology | Rabbit | 1:1000 | 2679s |
| β-actin | Sigma | Mouse | 1:5000 | 22190126/A5441 |
| **Secondary** | **Supplier** | **Dilution** | | |
| Polyclonal goat anti-mouse IgG | DAKO | 1:100 | | PO447 |
| Polyclonal goat anti-rabbit IgG | DAKO | 1:100 | | PO448 |
| **Tertiary** | **Supplier** | **Dilution** | | |
| Polyclonal rabbit anti-goat IgG (HRP) | DAKO | 1:100 | | PO449 |

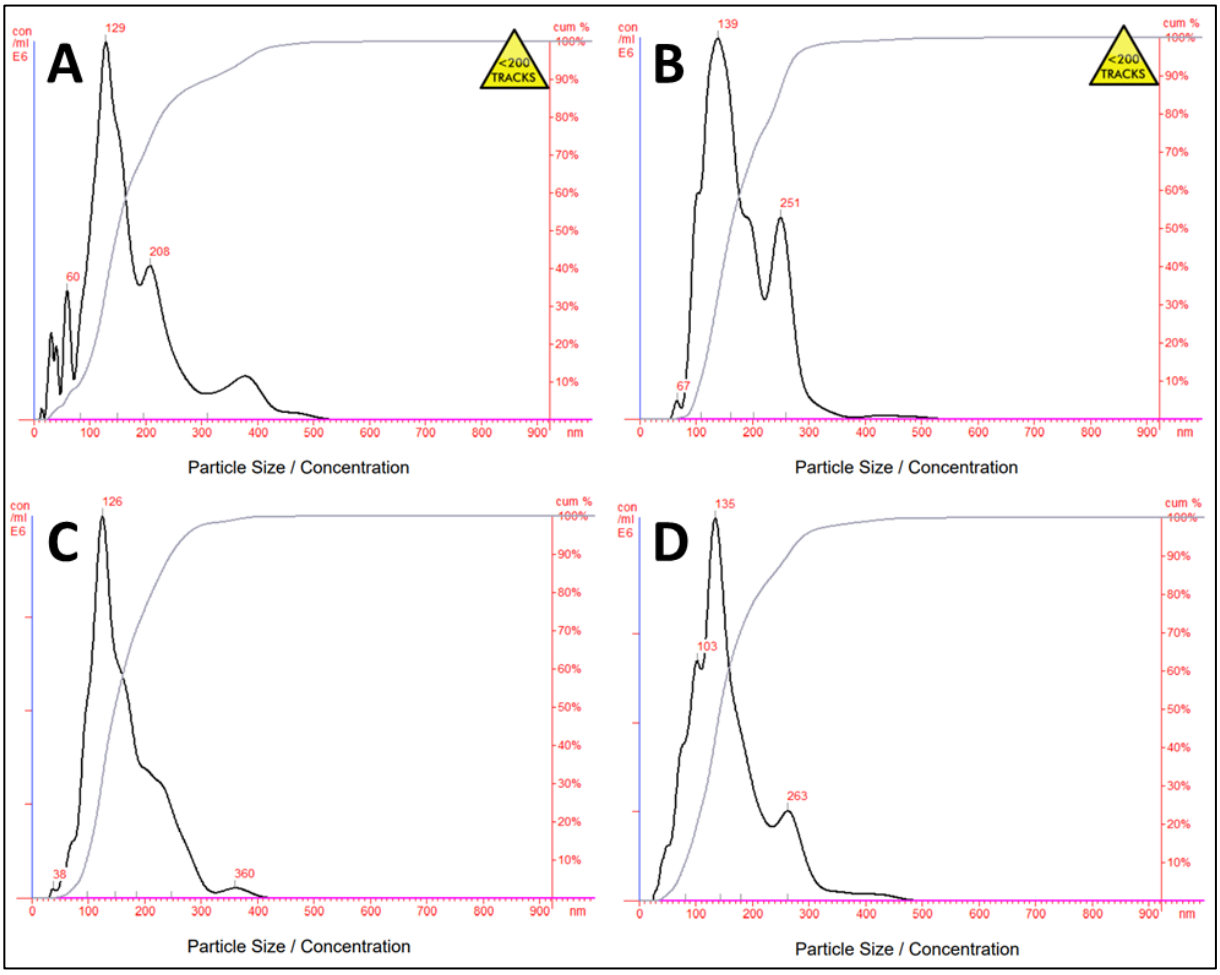


*Supplementary Figure 1: Particle size distribution plots obtained by NTA. (A) Starvation medium control. (B, C & D) Conditioned medium samples (expected to contain EVs). It can be seen that most particles lie in the size range 50-300nm.*

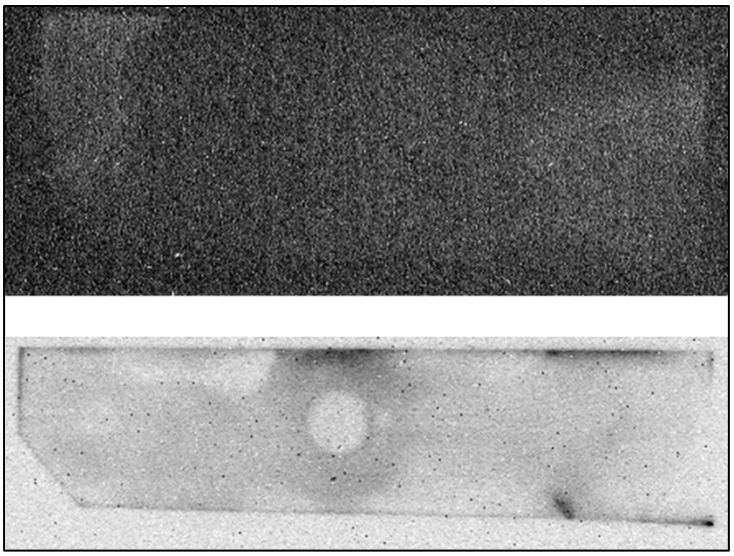

*Supplementary Figure 2: Empty Dot blot controls. (Top membrane) Membrane incubated with goat anti-mouse secondary antibody and rabbit anti-goat (HRP) tertiary antibody. (Bottom membrane) Membrane incubated with goat anti-rabbit secondary antibody and rabbit anti-goat (HRP) tertiary antibody. Bright circular spot was identified as an air bubble.*

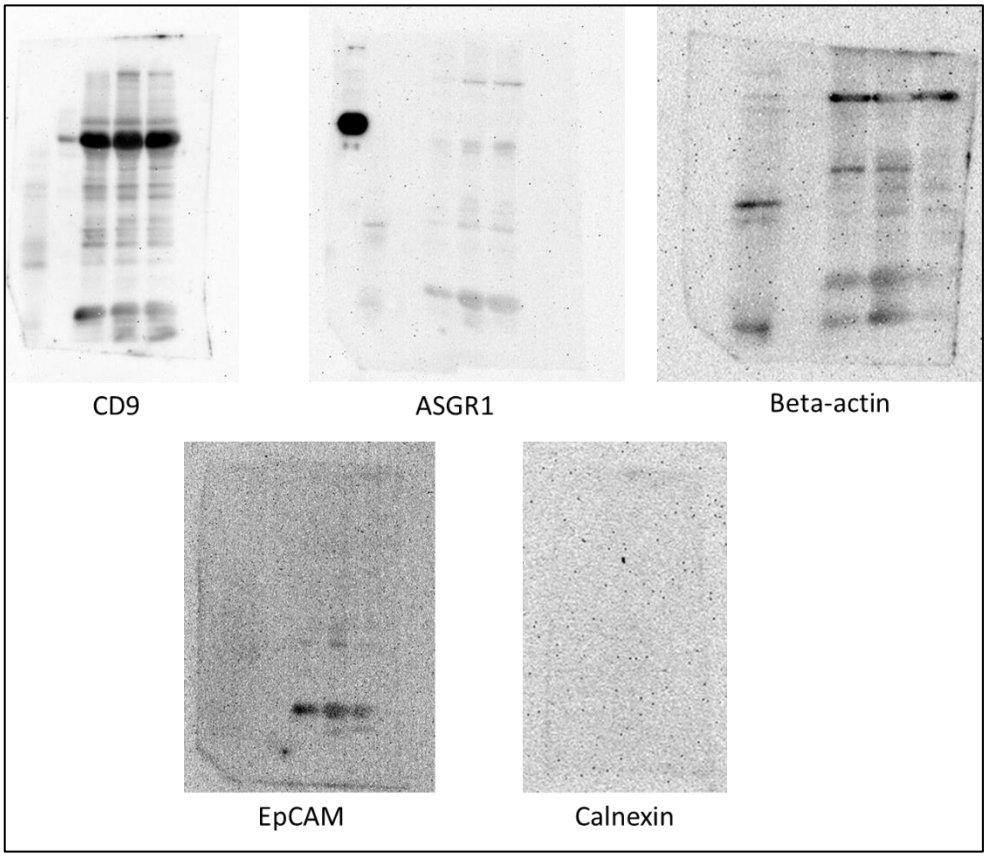


*Supplementary Figure 3: Western blot results showing entire blots of proteins CD9, ASGR1, β-actin, EpCAM and Calnexin. It can be observed that EpCAM and Calnexin proteins are not expressed, although the EpCAM blot does show some non-specific binding.*

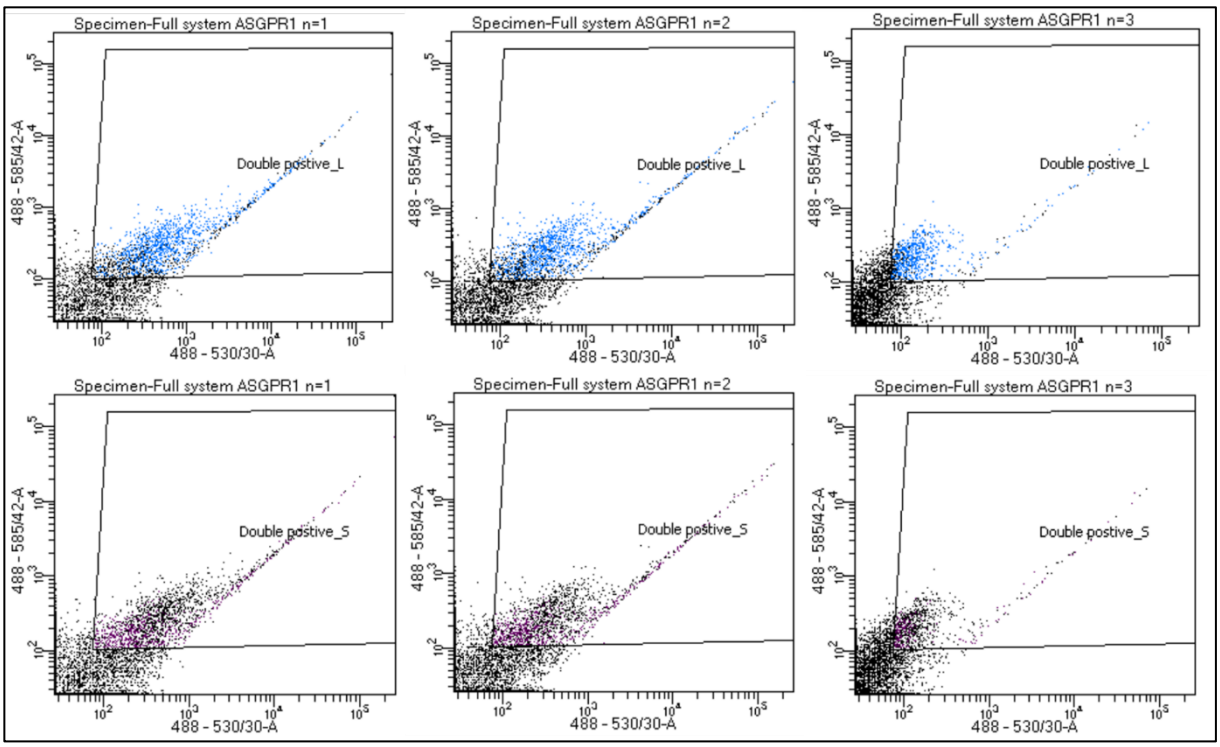


*Supplementary Figure 4: Results obtained with the "double positive" gating strategy when comparing double positive graphs between high f/s scattering beads (top three plots) and low f/s scattering beads (bottom three plots). The plots display that high f/s scattering beads are less often positive because they are on the diagonal line (indicating overlap of Pe and FITC channels) compared to low f/s scattering beads. This suggests that high f/s scattering beads are more "truly" positive for both FITC (due to Calcein) and Pe (due to Tz groups).*